International Journal of Biological Macromolecules

Structural and biochemical characterization of SmoPG1, an *exo*-polygalacturonase from *Selaginella moellendorffii*

Camille Carton[a], Josip Safran[a], Adrien Lemaire[a], Jean-Marc Domon[a], Ward Poelmans[b,c], Tom Beeckman[b,c], Francisco Ramos-Martín[d], Viviane Antonietti[e], Pascal Sonnet[e], Anissa Lounès – Hadj Sahraoui[f], Valérie Lefebvre[a], Jérôme Pelloux[a], Corinne Pau-Roblot[a*].

[a]UMRT INRAE 1158 BioEcoAgro – Biologie des Plantes et Innovation, Université de Picardie Jules Verne, UFR des Sciences, 33 Rue St Leu, 80039 Amiens, France
[b]Department of Plant Biotechnology and Bioinformatics, Ghent University, Ghent 9052, Belgium.
[c]Center for Plant Systems Biology, VIB-UGent, Ghent 9052, Belgium.
[d]Unité de Génie Enzymatique et Cellulaire UMR 7025 CNRS, Université de Picardie Jules Verne, F-80039 Amiens, France
[e]Agents infectieux, resistance et chimiothérapie (AGIR), EA4294, Université de Picardie Jules Verne, UFR de Pharmacie, 1, rue des Louvels, 80037 Amiens, France
[f]Unité de Chimie Environnementale et Interactions sur le Vivant (UCEIV), Université du Littoral Côte d'Opale, 50, Rue Ferdinand Buisson, 62228 Calais Cedex, France

*__Corresponding author :__ UMRT INRAE 1158 BioEcoAgro – Biologie des Plantes et Innovation, Université de Picardie Jules Verne, UFR des Sciences, 33 Rue St Leu, 80039 Amiens, France.

E-mail address: corinne.pau-roblot@u-picardie.fr (C. Pau-Roblot)

Abstract

Polygalacturonases (PGs) can modulate chemistry and mechanical properties of the plant cell wall through the degradation of pectins, one of its major constituents. PGs are largely used in food, beverage, textile, and paper industries to increase processes' performances. To improve the use of PGs, knowledge of their biochemical, structural and functional features is of prime importance. Our study aims at characterizing SmoPG1, a polygalacturonase from *Selaginella moellendorffii,* that belongs to the lycophytes. Transcription data showed that *SmoPG1* was mainly expressed in *S. moellendorffii* shoots while phylogenetic analyses suggested that SmoPG1 is an exo-PG, which was confirmed by the biochemical characterization following its expression in heterologous system. Indeed, LC-MS/MS oligoprofiling using various pectic substrates identified galacturonic acid (GalA) as the main hydrolysis product. We found that SmoPG1 was most active on polygalacturonic acid (PGA) at pH 5, and that its activity could be modulated by different cations (Ca^{2+}, Cu^{2+}, Fe^{2+}, Mg^{2+}, Mn^{2+}, Na^{2+}, Zn^{2+}). In addition, SmoPG1 was inhibited by green tea catechins, including (−)-epigallocatechin-3-gallate (EGCG). Docking analyses and MD simulations showed in detail amino acids responsible for the SmoPG1-EGCG interaction. Considering its expression yield and activity, SmoPG1 appears as a prime candidate for the industrial production of GalA.

Key words: Plant cell wall, Polygalacturonases, pectins, *Selaginella moellendorffii*

1. Introduction

The plant cell wall is a complex and dynamic network composed of polysaccharides and proteins [1]. The structure of the cell wall is continually modified during plant development in order to shape the different cell types that make up the tissues and organs [2]. The primary plant cell wall (PCW) is mainly composed of cellulose, hemicellulose and pectins [3]. Pectins are the major constituents of the primary cell wall, and play a crucial role in a number of developmental processes through their synthesis, modification, and degradation [4]. Pectins are composed of homogalacturonan (HG), xylogalacturonan (XG), rhamnogalacturonan I (RG-I) and rhamnogalacturonan II (RG-II) domains which differ in their composition and complexity [5]. HG is a linear homopolymer of α-(1→4)-linked D-galacturonic acid (GalA) residues that can be methyl-esterified at C-6 and acetyl esterified at O-2 and/or O-3. XG is an HG substituted at O-3 by xylose monomers or dimers. RG-I consists of a backbone of repeating diglycosyl units (→2)-α-L-Rhap-(1→4)-α-D-GalpA-(1→), partially substituted at O-4 positions of α-L-Rhap residues with various side chains such as (1→5)-α-L-arabinans; (1→4)-β-D-galactans; arabinogalactans type I (AGI) containing (1→4)-β-D-Galactan core with partial α-L-arabinans substitution and arabinogalactans type II (AG II) characterized by a

backbone of β-(1→3)-linked D-Gal*p* residues substituted at O-6 with single Gal*p* residues or with short chains of β-(1→6)-linked D-Gal*p* residues, which can in turn be substituted at O-3, O-4 and/or O-6, by Ara containing chains. RG-II is a complex substituted-HG encompasses thirteen different sugars and twenty one distinct glycosidic linkages arranged as a backbone formed by nine partially methyl-esterified GalA residues substituted by different side chains [6,7]

The degradation of pectins in the cell wall is regulated by different classes of pectin-modifying enzymes, referred to as pectinases [4]. These pectinases are also employed for example, in food, beverage, feed, textile, and paper industries, for modulating pectin content [8]. Among pectinases, polygalacturonases (PGs, GH 28) are largely represented and can be divided into two types depending on their structures and biochemical activities: endo-PGs (EC 3.2.1.15), cleave α-1,4-glycoside bonds between two non methyl-esterified galacturonic acid residues while exo-PGs cleave the α-1,4-glycoside bond at the non-reducing end in polygalacturonic chains of a pectin molecule [5,9]. Exo-PGs are further classified into two subclasses : i) class I, EC 3.2.1.67, galacturan 1,4-α-galacturonosidase release galacturonic acid residue while ii) class II, EC 3.2.1.82, exo-poly-α-galacturonosidase release digalacturonic acid [10].

Polygalacturonases from fungi [10–12] or bacteria [13,14] are well described in literature, highlighting their biochemical characteristics and specificities (substrate, pH, stability, etc…). However data related to the biochemical characterization of plant polygalacturonases are scarce including both endo-PGs [4,15] and exo-PGs [16,17].

Various industries such as textiles and leather, food and beverages, paper and pulp, wastewater treatment but also various applications in pharmaceutical, research and biotechnology diagnostics use enzymes. The enzyme market is expected to grow from USD 12.1 billion in 2022 to USD 16.9 billion in 2027 with a Compouned Annual Growth Rate as around 6.8% [18]. More precisely, PGs market is projected to growth from 2024 to 2031 from USD 15 million to USD 40 million. The growth of the market can be attributed to the increasing use of PG (approximatively 15% representing by exo-PG) in the food, feed industry, textile and biomass application [19]. PGs are highly efficient biocatalytic enzymes to the conversion of renewable pectic polysaccharide biomass into bioactive oligogalacturonides [8], to juice extraction and clarification, viscosity reduction, nutrient release and increased absorption in the feed industry and textile degumming [20,21].

Various studies have reported the use of bacterial, fungal and plant exo-polygalacturonases in industrial applications and during developmental processes. For example, exo-PG from *Penicillium janczewskii* or *Sporothrix schenckii* are used to improve viscosity, clarity and yield of apple, mango or peach juice [22,23]. Exo-PG from *Klebsiella* sp. Y1 reduces the viscosity

of PGA and facilitate nutrient absorption [24]. Only few of them reported on their biochemical and structural characterization and their mode of action [10,25]. Thus, to improve PGs' usability in several industrial processes, knowledge of their biochemical, structural and functional features is of prime importance [12,26].

In the present work, we characterized a novel PG from *Selaginella moellendorffii*. *Selaginella* (Selaginellaceae, order Selaginellales, class Lycopsida) is a monophyletic lycophyte genus, characterized by microphylls and adaxial reniform sporangia [27]. Species from the *Selaginella* genus possess a simple morphology and appearance and are widely present on all continents, except Antarctica. The availability of the *S. moellendorffii* genome sequence [28,29] now facilitates studies of their pectinases, in particular by allowing comparison with angiosperm PGs. We report on the first comprehensive phylogeny of *S. moellendorffii* polygalacturonases, as well as gene expression levels and a biochemical and structural characterization of SmoPG1, an exo-polygalacturonase. This enzyme showed activity in the 25-50°C range with a maximum activity at 45°C and pH 5. Besides, SmoPG1 was active and stable over a wide range of temperature and pH values, which can be of interest for biotechnological applications due to its functional properties. Biochemical tests with different ions and inhibitors shed new light on the regulation of SmoPG1 activity. Docking studies highlighted the rationale for the inhibition of SmoPG1 by (−)-epigallocatechin-3-gallate (EGCG) through fixation in the active site while molecular dynamics studies showed the importance of Asp and Glu residues in the affinity. These results suggest the potential effect of EGCG on PG activity regulation.

2. Material and Methods

2.1. Bioinformatic analysis and homology modelling

The initial genomic sequences of *S. moellendorffii* PGs were obtained using the available genome database (ftp.broadinstitute.org). Subsequently, these sequences underwent iteractive searches using NCBI and UniProt Blast until 30 PGs were retrieved. SignalP-5.0 server was used to predict the presence of putative signal peptide (http://www.cbs.dtu.dk/services/SignalP/) and NetOGlyc 4.0 / NetNGlyc 1.0 server to predict putative O- and N- glycosylation sites, respectively (http://www.cbs.dtu.dk/services/NetOGlyc/; http://www.cbs.dtu.dk/services/NetNGlyc/). Phylogenetic analysis was carried out using MEGA multiple sequence alignment program (https://www.megasoftware.net/) and sequence alignments were realized with ClustaOmega (https://www.ebi.ac.uk/Tools/msa/clustalo/). The structure of YePG was downloaded from PDB (2UVF). AtPGF10 and SmoPG1 models were downloaded from AlphaFold2 database, while UCSF Chimera (http://www.cgl.ucsf.edu/chimera/) was used for creation of graphics.

2.2. *SmoPG1* expression in *S. moellendorffii*

S. moellendorffii was propagated as described in Motte et al., 2022 [30]. Explants were generated by excising apical shoot segments with two to three branching points without any signs of root development. These explants were subsequently grown on standard ½ MS medium with 20 µm mesh nylon membranes (Prosep, Zaventem, Belgium) for 12 days in a growth chamber. To facilitate analysis and comparison of gene expression levels in different segments of these explants, 90 root tips, 30 shoot tips, 20 shoot segments between branching points or 50 root segments (Fig. 2B) were collected and pooled for RNA extraction. Total RNA was isolated using the ReliaPrep™ RNA Miniprep System (Promega, Madison, WI, USA) and complementary cDNA was synthesized from 0.75 µg RNA with qScript® cDNA SuperMix (Quantabio, Beverly, Massachussets, United State). The qPCR assays were performed with SYBR® Green Mix (Roche, Basel, Switzerland) in a LightCycler® 480 (Roche, Basel, Switzerland). Genes LOC9655921 and LOC9638502 were used as reference genes. Relative expression levels were calculated using qbase+ (www.qbaseplus.com).

2.3. Cloning and heterologous expression of SmoPG1

The gene sequence of *S. moellendorffii* SmoPG1 (Uniport: D8TDH2) was synthesized as a codon-optimized version for *Pichia pastoris* yeasts, without peptide signal, in pPCIZ-αB plasmid (ProteoGenix, Schiltigheim, France) in frame with a His-tag, using Pst1 and Not1 restriction sites. This vector was used for transformation of *E. coli* TOP10 (Invitrogen, Waltham, Massachussets, United State). Clones carrying vector were selected using Zeocine (C=25 µg/mL), and verified with colony PCR AOX primers (Invitrogen, Waltham, Massachussets, United State) and grown in LB low salt (1 % peptone, 0.5 % yeast extract, 0.5 % sodium chloride). Plasmids were purified using High Purity Plasmid Miniprep (NEoBiotech, Évry-Courcouronnes, France) and the linearized vector was used to transform *Pichia pastoris* X33. The positive clones were selected on zeocin (C=100 µg/mL) in Yeast extract Peptone Dextrose media (1 % yeast extract, 2 % peptone and 2 % dextrose).

2.4. Production and purification of the recombinant SmoPG1

SmoPG1 was produced in *P. pastoris* following the protocol described by Lemaire *et al.*, 2020 [31]. The yeast cells were grown at 30°C on buffered glycerol-complex medium (1 % yeast extract, 2 % peptone, 100 mM potassium phosphate pH 6, 1.34 % YNB, 4×10^{-5} % biotin and 1 % glycerol) in baffled flasks. After 24 h, the cells were transferred in buffered methanol-complex medium without glycerol, with a final concentration of 0.5 % of methanol. The methanol concentration was maintained by adding 2 mL of 25 % methanol to 100 mL of culture every 24 h to maintain a final concentration of 0.5 % in the medium during 72 h [31].

The culture was then centrifugated (1,500 g, 10 min, 4 °C) and filtered with GD/X 0.45 µm PES filter Media (Whatman, Maidstone, United Kingdom).

The purification of SmoPG1 was performed using 1 mL HisTrap excel column (GE Healthcare, Chicago, Illinois, United State). The column was first equilibrated with 10 volumes of equilibration buffer (50 mM NaP pH 7.2, 250 mM NaCl). 100 mL of the supernatant culture was loaded in the column at 1 mL/min flow rate. HisTrap column was washed with 10 column volumes of wash buffer (50 mM NaP pH 7.2, 250 mM NaCl, 5 mM imidazole). The recombinant protein was recovered after addition of 10 column volumes of elution buffer 1 (50 mM NaP pH 7.2, 250 mM NaCl, 25 mM imidazole) followed by 10 column volumes of elution buffer 2 (50 mM NaP pH 7.2, 250 mM NaCl, 100 mM imidazole). SmoPG1 was concentrated using Amicon Ultra Centrifugal filter with a 10 kDa cut-off (Merck Millipore, Burlington, Massachusetts, United States). SmoPG1 buffer exchange was performed in McIlvain buffer pH5 [32] with PD Spintrap G-25 column (GE Healthcare, Tremblay-en-France, France).

Protein concentrations were determined by Bradford test using Bovine Serum Albumin (A7906, Sigma-Aldrich, Saint-Quentin-Fallavier, France) as standard. Purity molecular weight and glycosylations were estimated by electrophoresis with the protocol described by Lemaire *et al*., 2020 [31]. SmoPG1 was deglycosylated with the peptide-N-glycosidase F at 37 °C for 1 h according to the supplier's instructions (New England Biolabs, Évry-Courcouronnes, France) and then analysed by SDS-Page.

2.5. Enzyme activity

The activity of purified SmoPG1 was determined using the DNS method [33]. 3 µg of purified SmoPG1 in McIlvain buffer at pH 5 was incubated with PGA (81325, Sigma-Aldrich, Saint-Quentin-Fallavier, France) at a final concentration of 0.4 % at 50 °C for 30 min. Each enzymatic measurement was performed in triplicate.

The optimal temperature for activity was determined between 25 °C and 60 °C by measurement of SmoPG1 activity with PGA (final concentration: 0.4 %) after 30 min of incubation. The thermostability of SmoPG1 was assayed by pre-incubating the enzyme for 30 min between 25 °C and 60 °C, after which the SmoPG1 activity was measured at optimal temperature.

The optimal pH activity of SmoPG1 was determined between pH 4.0 to 8.0 at 50 °C, according to the conditions previously described. The pH stability of SmoPG1 was determined by pre-incubating the enzyme at ambient temperature for 90 min at pH between 4 to 8, after which the PG activity was determined according to the conditions previously described.

The effects of different substrates on SmoPG1 activity were determined at pH 5, 50 °C for 120 min using substrates (0.4 % final) with different degree of methyl-esterification (DM) and acetylation (DA): polygalacturonic acid noted PGA (81325, Sigma-Aldrich, Saint-Quentin-Fallavier, France), citrus pectins with DM 55 to 70 % (P94436, Sigma-Aldrich, Saint-Quentin-Fallavier, France), citrus pectins with DM 71% (Cargill, Puteaux, France), sugar beet pectin with DM 42%, and DA 31% (Cargill, Puteaux, France) and apple pectin with DM 70 to 75 % (76282, Sigma-Aldrich, France). The effects of metal ions on SmoPG1 activity were determined by the addition of various metal ions: Ca^{2+}, Cu^{2+}, Fe^{2+}, Mg^{2+}, Mn^{2+}, Na^{2+}, Zn^{2+} at 1 mM in the reaction medium. The activity was measured by the DNS method with the conditions previously described.

Different chemical compounds were tested on SmoPG1 activity by incubating 6 µg of purified enzyme with Polyphenon 60 at 1.25 mg/mL (PP60, #P1204, Sigma-Aldrich, France), tannic acid 0.002 mg/mL and 0.02 mg/mL (TA, #403040, Sigma-Aldrich, France) and (−)-epigallocatechin-3-gallate at 0.5 mg/mL (EGCG, #E4143, Sigma-Aldrich, France), with PGA at 0.4 % final. The activity was measured by the DNS method with the conditions previously described, and an incubation time of 60 min.

2.6. Kinetic parameters

The K_m and V_{max} values of SmoPG1 were determined using 4 µg of purified enzyme at 50°C in McIlvain buffer pH 5 with concentrations of PGA between 0 and 9 mg/mL and incubation time of 20 min. The kinetic parameters were calculated using Prism - GraphPad 8.

2.7. SmoPG1 circular dichroism spectra

Circular dichroism (CD) spectra were obtained in the far-UV (260–195 nm) using a J-815 Jasco spectropolarimeter (Jasco, Lisses, France). The CD measurements were performed at 45 °C and 60 °C, using a 1 mm path cell, with 3 accumulations for all samples in McIlvain buffer pH 5. Temperature was controlled using a PFD-425S Peltier-type heating system. All proteins were subjected to CD analysis at a concentration of 18 µM. The secondary structure was determined by CD Multivariate Secondary Structure Estimation (SSE) program (Jasco, Lisses, France), using the principal components regression (PCR) and partial least square (PLS) multivariate method.

2.8. Docking analyses of SmoPG1-EGCG complex

SmoPG1 (receptor) models were retrieved from AlphaFold2 database while structure of epigallocatechine-3-gallate (EGCG, ligand) was downloaded from the pH1N1 2009 polymerase subunit PA endonuclease (PDB: 4AWM). To understand the inhibition of SmoPG1 by EGCG, AutoDock4 was used for protein–ligand docking [34]. To generate the input files for EGCG and SmoPG1 AutoDock tools were used to add charges, merge non-

polar hydrogens, and assign appropriate atom types. Molecules were saved in ".pdbqt" file format. A cubic grid 68 Å x 84 Å x 76 Å around the active site was built by the Autogrid program. Grid point step 0.375 Å was taken. The 12 non-cyclic σ bond torsions of the EGCG molecule were free to rotate. A Lamarckian genetic algorithm and default parameters with 50 docking runs were used in AutoDock4 docking. This process was repeated four times. The three best docked conformation from each run, twelve in total, with lowest energy (-kcal/mol), were analysed with Chimera [35].

2.9. MD simulation of SmoPG1-EGCG complex

MD simulations were carried out with the GROMACS molecular dynamics package [36] with the CHARMM36m force field [37]. CHARMM-GUI Solution Builder [38] was utilized to create the simulation setups using the structure that was acquired from the docking experiments. EGCG was modeled by CHARMM-GUI "Ligand Reader & Modeler" [39] and parameterized by Antechamber [40,41]. TIP3P molecules [42] were extended 10 Å from the protein. Charges were neutralized with Na^+ counterions. Periodic boundary conditions were employed using the NPT ensemble with a constant pressure of 1 atm and a temperature of 310 K. The Particle Mesh Ewald (PME) method was used for long-range electrostatic interactions. Each system was energy-minimized with a 5000-step steepest-descent algorithm. The Parrinello-Rahman barostat [43] was used to maintain pressure (1 bar) isotropically with a time constant of 5 ps and a compressibility of 4.5×10^{-5} bar^{-1}. Nose-Hoover thermostat [44,45] with a time constant of 1 ps was chosen to maintain the temperature. All bonds were constrained by the LINear Constraint Solver (LINCS) algorithm [46]. After minimization and equilibration, 250 ns were simulated for production. The whole process was performed three times for reproducibility. GROMACS tools were used to analyse the MD trajectories. Polar contacts were determined by calculating the radial distribution functions of each nitrogen and oxygen atom in relation to all others and taking its maximum intensity in the range of H-bonds and salt bridges [47]. The trajectories were visualized and eventually turned into a video using VMD [48].

2.10. Profiling of oligogalacturonides released from commercial pectins

The activity of SmoPG1 was assessed using pectic substrates of various DM and DA. Oligogalacturonides (OGs) released after digestions by SmoPG1 were identified by the LC-MS/MS method described by Voxeur et al., 2019 [49]. PGA (81325, Sigma-Aldrich, France) and citrus pectin of DM 55–70% (P9436, Sigma-Aldrich, France) were used at a final concentration of 0.4 % (w/v) in 50 mM ammonium acetate buffer (pH 5) and incubated with 10 µg SmoPG1 in 100 µL final volume for 2h, 6h and overnight at 40 °C. The reaction was stopped with addition of 1 volume of 100 % ethanol and non-digested pectin were pelleted by centrifugation (5,000 g, 5 min). The supernatant was dried in a speed vacuum concentrator

(Concentrator plus, Eppendorf, Hamburg, Germany). The OGs were suspended in 200 µL of LC/MS water. Separation and identification of OGs were done as previously described by Safran et al., 2023 [25].

3. Results and discussions:

3.1. Sequence, phylogeny analysis

To asses phylogenetic relationship of *S. moellendorffii* PGs, 30 SmoPGs were retrieved from NCBI and UniProt databases with addition of 5 PGs, 2 endo-PGs and 3 exo-PGs, from *Arabidopsis thaliana* and two exo-PGs from *Yersinia enterocolitica* and *Bacillus licheniformis* to create a phylogenetic tree (Fig. 1A). The comparison between *S. moellendorffii* protein sequences show that all SmoPGs are grouped in pairs. The sequences of SmoPGs showed high sequences identity (45.2 to 100 %). For example, SmoPG1-PG6 share 98.5 % identity, SmoPG2-PG3: 97.95 %, SmoPG12-PG13: 98.5 %, and SmoPG10-PG15: 97.61 % (Table S1). These sequence similarities are explained by the fact that the assembled genome includes two haplotypes that are 98.5 % identical at the nucleotide level [28] and indicate that *S. moellendorffii* is diploid.

Insert Fig.1

Two clusters of PGs can be distinguished: one corresponding to putative exo-acting enzymes and the second one to endo-polygalacturonases from plants and bacteria, sharing low sequence identity (Fig. 1A). Analysis showed sequence identities of 44 %, 44 % and 43 % between SmoPG1 (red star) and *A.thaliana* exo-polygalacturonases AtPGF7, AtPGF12 and AtPG10, respectively [16]. Moreover, within this cluster (orange cluster, Fig 1A), PGs with similar structures and processivities can be found as indicated by high sequence identity, between 40 to 50% (Table S1). It has to be noted that SmoPG1 belongs to this cluster, making it a probable exo-PG. In the second cluster (blue cluster, Fig. 1A), two polygalacturonases of *A. thaliana* have been listed: ADPG2 and PGLR, which were characterized as endo-polygalacturonases and showed high sequence identity with SmoPG15 (43 % and 42.89 %, respectively) and in comparison, low sequence identity with SmoPG1 (26.98 % and 26.01 %, respectively) [25]. These results therefore suggested that the second cluster, which includes SmoPG15, corresponds to endo-polygalacturonases. The last cluster contains PGs from bacteria (BlPG and YePG), listed in the literature as exo-polygalacturonases, and four SmoPGs (SmoPG4; SmoPG19, SmoPG8 and SmoPG29) [50,51]. BlPG and YePG shared low sequence identity with SmoPG1 (31 % and 24 %, respectively) which could indicate a particular structure of theses PGs. However, the 4 four SmoPGs in this cluster also shared low sequence identity with BlPG (~23 %) and between

24 and 26 % with YePG, which did not allow us to speculate on a possible mode of action for these SmoPGs, but we can assume their structures to be similar with bacterial PGs.

3.2. Homology modelling strongly supports SmoPG1 as an exoPG

Modelling of SmoPG1 with Alphafold2 highlighted the presence of conserved β-helical structure (Fig. 1B), which is a fold characteristic of pectinases [52]. This β-helix is formed by four β–sheets with different numbers of β-strands in each sheet. SmoPG1 also showed a α-helix at the N-terminus, protecting the hydrophobic core of the enzyme. Sequence alignment and structural superposition of SmoPG1 (Fig. 1C, Fig. S1), with AtPGF10 [16] (43 % identity) and YePG [51] (24 % identity), two polygalacturonases characterized as exo-acting enzymes, showed high structural conservation between the PGs even if they have low sequence identity. One particular feature resides in the presence of an additional loop closing the binding groove, which appeared specific to exo-PG and absent of all endo-PG's structure (Fig. S2) determined so far [51]. This loop, consisting of W126 to L149, seals off the active site where the non-reducing end of the sugar is accommodated. Active site of SmoPG1 (Fig. 1D) harboured 3 aspartic acids (D239, D260, D261) with other amino acids (asparagine (N237), arginine (R326) and lysine (K328)) forming the 3 conserved motives (NTD, DD, RIK) previously found in polygalacturonases.

3.3. SmoPG1 is expressed in *S. moellendorffii* shoots and to a lesser extent than in roots

Using the publicly available RNA-seq data, the expression of all polygalacturonase genes was assessed using CoNekT [53]. The important sequence similarity that exists between each pair of paralogs does not allow distinguishing the expression of either of the gene's pairs. Therefore, expression data for only 15 different accession numbers, each corresponding to a pair of polygalacturonases, could be retrieved and compared [54]. Heat-map showed that exo-PGs, including atypical exo-PGs more similar in sequence to bacterial ones, present a higher expression level than putative endo-PGs. Indeed, the most highly expressed gene clusters are coding for exo-PG (SmoPG12-PG13 and SmoPG4-PG19). Both showed the highest expression level in aerial tissues. This observation seems counter-intuitive when considering the more prominent cell-wall modifications that can result from endo-PG activity. Results presented in Fig. 2A showed that *SmoPG1-PG6*, corresponding to the expression of both SmoPG1 (D8RQ82)– and – SmoPG6 (D8TDH2)– coding genes, is the third most expressed PG cluster and constitutively expressed in all organs and physiological conditions present in the dataset, albeit to a relatively low level. We further confirmed that *SmoPG1* is expressed both in roots and shoots, as determined by RT-qPCR from *S. moellendorffii* tissues grown under our standard conditions (Fig. 2B, C). The

expression levels of *SmoPG1* in the shoot tips were 1.5 times higher than those of the differentiated root tissue, and 1.35 times higher in the shoot compared to the differentiated root tissue. No statistically significant difference in expression was otherwise detected. While available data on *PG* gene expression are scarce, these results suggest the putative role of SmoPG1 in growing and developing tissues of *S. moellendorffii*.

Insert Fig.2

3.4. SmoPG1 expressed in Pichia harboured a typical PG-fold

The analysis of the SmoPG1 sequence showed that the protein is composed of 468 amino acids harbouring a putative signal peptide at the N-terminus and putative N- and O-glycosylation sites: 9 and 7, respectively (Table S2). After removal of the signal peptide, a 442 amino acids sequence, with a predicted molecular mass of 48 kDa, was expressed in *Pichia pastoris*. The produced protein possessed c-Myc and 6 x His tags fused to its C-terminus end, the latter being used for affinity chromatography purification. After successful production and purification (Fig. 3A), a band of a molecular mass of ~72 kDa was detected (Fig. 3A, lane 2). To assess if the size shift was related to extensive glycosylation by *Pichia pastoris*, the protein was deglycosylated using PNGase F (Fig. 3A, lane 1). The molecular mass of the protein after deglycosylation shifted to 55 to 60 kDa, which is in line with the predicated size of the protein harbouring the His and c-Myc tags as well as the presence of putative O-glycosylation sites.

Insert Fig.3

The thermal stability and secondary structure analysis of SmoPG1 were assessed by circular dichroism (CD) (Fig. 3B). The CD spectra from SmoPG1 were obtained at 20 °C, 45 °C and 60 °C, temperatures at which polygalacturonases are usually active [1,16,55]. Spectra showed a secondary structure with an abundance of β-sheet, in particular at its optimal activity temperature, 40.5 % and 36.3 % estimated with the PCR and PLS methods, respectively, and a low abundance of α-helix with 3.5 % and 4.5 %, respectively. These results are typical for polygalacturonases which are mainly composed of parallel β-sheets forming a right-handed β-helical structure [25,56–58]. In Fig. 3B, we can observe that the secondary structure is generally conserved in this temperature range, mainly for β-sheets, turns and irregular structures. For α-helix, we observed a loss of structure from 12 % and 14.7 % at 20 °C to 3.5 % and 4.5 % at 45°C. This decrease might be explained by the loss of β-sheet and irregular structures, and by the changes of turns conformation containing α-helix around the active site (Fig. 3B) [59].

3.5. SmoPG1 is bona fide polygalacturonase

We next tested the activity of SmoPG1 on various pectic substrates that differ in their methyl-esterification and acetylation degrees (Fig. 3C). The maximum activity was measured using polygalacturonic acid (PGA) after 120 min of incubation, while only 0 to 3 % of residual activity was detected when using citrus pectins with degrees of methylation (DM) from 55 to 70 %, sugar beet pectins DM with 42 % and degree of acetylation (DA) 31 %, or apple pectins with DM 70 to 75 %. Therefore, SmoPG1 activity was strongly affected by the degree of methyl-esterification of the substrate, and even more by the degree of methyl/acetyl esterification, as sugar beet pectin substrate showed the lowest activity (Fig. 3C). The reduction of SmoPG1 activity with increased DM has also been observed for other endo-PGs [1,60,61] and exo-PG [50] from plants, insects, fungi and bacteria.

Characterization of temperature and pH optima were then performed using PGA as substrate. The optimal temperature and the thermostability were determined after 30 min reaction in McIlvain buffer pH 5, between 25 and 60 °C. SmoPG1 exhibited the highest activity at 45 °C (Fig. 3D) and was relatively stable between 35 and 50 °C (about 80% of relative activity), whereas activity decreased sharply from 55 °C onwards (Fig. 3D). The optimal pH and the pH stability of the enzyme were tested in McIlvain buffer at pH 4.0 to 8.0 at 50 °C during 30 min (Fig. 3E). Data showed that the pH for optimal activity of SmoPG1 was 5. These results are in accordance with those described for an exo-PG from papaya (*Carica papaya*) whose optimum pH was 4.6 and optimum temperature was 45 °C [62], PGLR, an endo-PG from *A. thaliana,* whose optimum pH was 4 and optimum temperature was 50 °C [63] and VdPG2, an endo-PG from *Verticillium dahliae*, whose optimum pH was 5 and optimum temperature was 50 °C [55].

The stability of the enzyme over a wide pH range is an important enzymatic property for industrial applications. It was assessed by measuring the residual SmoPG1 activity after 90 min pre-incubation at ambient temperature with pH ranging from 4 to 8. SmoPG1 showed an increase in activity from pH 7 to more alkaline pH (Fig. 3E). Similar results were reported for an exo-PG from *Bacillus licheniformi*s, which was stable in a pH range from 5 to 10 [50].

The kinetic parameters of SmoPG1 were then determined using PGA as a substrate and under the favourable conditions (50 °C and pH 5). K_m and V_{max} were 7.310 mg.mL^{-1} and 1.793 nmol of GalA.min^{-1}.µg^{-1} of proteins, respectively (Fig. 3F; Table S2). The substrate affinity of exo-PGs varied according to the origin of PGs. For example, exo-PG of *B. licheniformis* has a K_m of 3.25 mg.mL^{-1} [50], exo-PG of *Neosartorya glabra* has a K_m of 6.9 mg.mL^{-1}[10] and papaya exo-PG has a K_m of 0.88 mg.mL^{-1} [62]. In comparison with endo-PGs, these values are comparable, for example VdPG2 has a K_m of 3.27 mg.mL^{-1} [55] or a PG of *D. abbreviatus L*. (DaPG) has a K_m of 3.68 mg.mL^{-1} [64]. The V_{max} of SmoPG1 were close to the values from exo-PGs from peach: 0.5 nmol of GalA.min^{-1}.µg^{-1} of proteins [65]. In

comparison with plant endo-PGs, the values are in the same order: 11 and 30,8 nmol of GalA.min^{-1}.µg^{-1} of proteins for ADPG2 and PGLR respectively [25].

3.6. SmoPG1 is an exo-acting enzyme, releasing GalA as main digestion product

To determine the mode of action of SmoPG1, non-esterified polygalacturonic acid (PGA) and citrus pectin DM 55-70 %, were digested with SmoPG1 during two and twelve hours. The digestion of these substrates led to the production of oligogalacturonides (OGs) which allowed determining the mode of action of SmoPG1. The analysis of the OGs produced was carried out by LC-MS/MS following the method of Voxeur et al., 2019 [49]. After PGA digestion, we identified galacturonic acid (GalA1) as the main hydrolysis product (~ 60 to 70 %) while trigalacturonic acid (GalA3 < 20 %) and oligogalacturonides with degree of polymerisation (DP) 6 (GalA6 < 10 %) were also detected (Fig. 3G). It is important to note that almost all the other OGs (DP 3 to 8) disappeared for the overnight incubation, suggesting that SmoPG1 cleaved the same homogalacturonan several times for PGA and produced only GalA1 (Fig. 3G). The detection of these OGs can be explained by a natural degradation of the substrate during the incubation as is suggested by Celorio-Mancera et al., 2009 and Morris et al, 2010 [66,67]. For the digestion of citrus pectin with DM 55 to 70 %, GalA1 was the main product for the two incubation times (Fig. 3H). The detection intensity showed that when the substrate is more complex (with methyl-esterification), the production of OG is drastically reduced and GalA1 was the main product for the two incubation times (Fig. 3H). The reduction of SmoPG1 activity with increased DM had also been observed for other endo-PGs [1,60,61] and exo-PG [50] from plants, insects, fungi and bacteria. Moreover, an increase in the proportion for the produced OGs after the overnight digestion with the two substrates was observed, and finally, LC-MS/MS analysis confirmed that SmoPG1 is an exo-PG from class I, able to release only GalA1 products.

3.7. Inhibition of SmoPG activity

In addition, the effects of metal ions on SmoPG1 activity were investigated (Table 1). Results showed that ions like Cu^{2+}, Mg^{2+}, Mn^{2+}, Na^{2+} and Zn^{2+} increased its activity by 23 %, 29 %, 33 %, 46 % and 68 %, respectively. In contrast, decreases in activity by ~54 % and 32 % were observed with Ca^{2+} and Fe^{2+}, respectively. Some of these results are in agreement with the exo-PG AtPGF10 where Mg^{2+} and Mn^{2+} ions induced an increase of 150 % and 100 % of the enzyme activity, however the opposite was observed for Zn^{2+} and Cu^{2+} [16]. These results are not in agreement with those obtained for various fungal PGs (*Penicillium oxalicum,* PoPG (endo-PG), *Mucor circinelloides,* McPG (endo-PG)*)* [60,68] and bacterial (*Bacillus licheniformis*, BlPG (exo-PG)) [50]. For example, Mn^{2+} improved SmoPG1 activity by 33 % whereas it decreased BlPG and PoPG activities [50,60]. It should be noted that Zn^{2+} was the ion that increased most the activity of SmoPG1. It therefore seems that the effects of these

metal ions are specific to each PG isoform. To summarise, the effects of various metal ions on SmoPG1 activity highlights the specificity of these interactions, with some ions enhancing activity while others exhibit inhibitory effects, highlighting the intricate regulatory processes governing enzyme function.

Insert Table 1

Finally, the effects of various chemical inhibitors of PME activity such as tannic acid, (−)-epigallocatechin-3-gallate (EGCG) and Polyphenon 60 (PP60) were assessed on the activity of SmoPG1 (Fig. 4A). Tannic acid was able to inhibit SmoPG1 activity by 89 % at 0.02 $mg.mL^{-1}$ and by 73 % at 0.002 $mg.mL^{-1}$. Comparable results were obtained when studying PGLR from *A. thaliana* [1]. EGCG at 0.5 $mg.mL^{-1}$, induced an inhibition of 81 % of the activity whereas, for PP60 (1.25 $mg.mL^{-1}$), a total inhibition of the activity was observed (Fig. 4A). Again, results were comparable to those of PGLR, 53 % inhibition for EGCG and 20.7 % for PP60) [1]. Previous studies reported that PP60 and EGCG can inhibit PME activity [1,61,69,70] as the inhibitory effect of EGCG was demonstrated on orange (CsPME), Arabidopsis (AtPME31), insect (*Sphenophorus levis*, Sl-PME) and tomato PME [32,38,39]. These results suggest that EGCG is not only an inhibitor of PMEs from plants [70] and fungi [69], for which it was initially characterized, but also an inhibitor of PGs. Furthermore, EGCG inhibitory effect is not only limited to pectinases but was also reported for a broad spectrum of biological processes, including interaction with epidermal growth factor signalling, prions, SARS-CoV-2 and other pectinases [69–71]. New studies should consider EGCG as a general inhibitor of plant pectin remodelling enzymes, including PMEs and PGs and that the negative effect observed on *A. thaliana* root development cannot be solely attributed to PME inhibition. [72].

Insert Fig 4

3.8. EGCG inhibition unveiled by docking studies and MD simulation

To further understand the rationale for such inhibition, docking studies were performed for the SmoPG1-EGCG complex to pinpoint the possible interaction between the enzyme and the ligand. Molecular docking analysis of EGCG and SmoPG1 showed that EGCG preferentially localizes in the active site cleft of SmoPG1 (Fig. 4B). More precisely binding energy values (ΔG), calculated for 200 different docking positions, ranged from -7.6 to -2.8 kcal/mol. The average ΔG for the best EGCG-SmoPG1 interaction was -7.3 kcal/mol. In comparison, the docking studies of EGCG with carrot PME showed ΔG values ranging from -6.37 to -3.38 kcal/mol [70]. The binding of EGCG is characterized by ligand–protein interaction between the catalytic amino acids and residues in the proximity of the active site with preferred, but not limited to, interaction with Asn and Arg (Table 2). The H-bonds

interaction, observed with EGCG with highest binding energy of -7.6 kcal/mol, showed interactions with R139, W212, G259, E303, D362 and catalytic site residues N237 and R326 (Fig. 4C). The same was observed with carrot PME where catalytic residues D136, W252 and W227 and residues Q113 and E253 located in the vicinity of the active site interacted with EGCG [70]. These docking results point to potentially key amino acids for the SmoPG1-EGCG interaction, thus mediating the inhibition of the activity of the enzyme. To study this in more detail, we have performed MD simulations. By using them, we can investigate the binding stability of docked EGCG in greater detail. We can also assess which residues are most important for the interaction over certain period of time. To achieve this, we ran three separate 250 ns long MD simulations (Supplementary data: SmoPG1-EGCG MD movie). In all of the repetition, EGCG predominantly remained within the active site or in its vicinity, effectively obstructing the entry of the substrate. However, we have also observed that EGCG can occasionally leave the active site and interact with the same charged amino acids, (mostly Asp and Glu), typically present inside the active. Future studies will evaluate more in detail the nature of the interaction in the presence of multiple EGCG molecules, a situation closer to the experimental conditions. These results are in accordance with observed biochemical data (Fig. 4A) where 19 % of SmoPG1 activity was still found at an ECGC concentration of 0.5 mg/mL. EGCG does not covalently bind to SmoPG1 but rather that its polar nature allows it to interact with active sites of enzymes from multiple families accounting for its known promiscuity regarding inhibiting similar enzymes, as mentioned before.

Insert Table 2

4. Conclusion

In conclusion, we have successfully purified and characterized a novel exo-polygalacturonase from *S. moellendorffii.* We showed that *SmoPG1*, is the third most expressed PG and constitutively expressed in all organs and physiological conditions present and that SmoPG1 was most prominently expressed in the plant shoot tips of *S. moellendorffii* pointing out its importance in plant development. Biochemical characterization showed that SmoPG1 had characteristics similar to previously characterized PGs, including an optimum acidic pH (5) and temperature (45°C). Sequence and phylogeny analysis with homology modelling suggested that SmoPG1 would be an exo-PG, which was confirmed by the LC-MS/MS analysis of released OGs where mainly galacturonic acid was produced confirming that SmoPG1 is an exo-PG. The effect of different ions on SmoPG1 activity was interesting, Zn^{2+} induced 68 % increase in activity, while Ca^{2+} and Fe^{2+}decreased the activity. We further showed that tannic acid, PP60 and EGCG have inhibiting effects on SmoPG1 activity with PP60 completely abolishing the activity. Docking studies could relate the inhibiting capacity

of EGCG to its interaction within the active site of SmoPG1, impairing substrate hydrolysis, while MD simulations confirmed that EGCG is preferentially binding to the active site thanks to the strong interaction with charged amino acids. Contrary to the previous results, EGCG is not only inhibiting PME activity, but it can also target other pectinases. This should be taken into consideration when testing for exogenous application of EGCG on plants. Taken together, the findings obtained from the biochemical characterization and the structural mass spectrometry data identify SmoPG1 as a potential tool for biotechnological applications in several industrial fields such as juice clarification or GalA production. The limit of the use of this enzyme is, since SmoPG1 is an exo-PG and it only releases GalA during its action on pectins, it cannot be used to produce bioactive oligosaccharides.

Funding sources:

This work was supported by: Conseil Regional Hauts-de-France, Université de Picardie Jules Verne, Université du Littoral Côte d'Opale, CPER BiHauts Eco de France, and Alliance A2U (Artois, ULCO, UPJV) through a PhD grant awarded to Camille Carton.

Acknowledgments:

The authors would like to acknowledge Serge Pilard from the "Plateforme Analytique de l'Université de Picardie Jules Verne" (Amiens, France) to LC-MS/MS experiments. We would like to thank the MatriCS platform (UPJV, Amiens, France) for computing resources.

Credit authorship contribution statement:

Camille Carton: Conceptualization, Data curation, Formal analysis, Investigation, Methodology, Writing - original draft. **Josip Safran:** Conceptualization, Formal analysis, Investigation, Methodology, Writing - original draft. **Adrien Lemaire**: Formal analysis, Investigation, Methodology. **Jean-Marc Domon:** Conceptualization, Investigation, Methodology. **Ward Poelmans:** Formal analysis, Investigation, Methodology. **Tom Beeckman:** Conceptualization, Investigation, Methodology**. Francisco Ramos-Martín:** Formal analysis, Investigation, Methodology. **Viviane Antonietti:** Conceptualization, Investigation, Methodology. **Pascal Sonnet:** Conceptualization, Investigation, Methodology. **Anissa Lounès – Hadj Sahraoui:** Funding acquisition**,** - Writing - review & editing. **Valérie Lefebvre:** Investigation, Methodology, Conceptualization, Writing - review & editing. **Jérôme Pelloux:** Conceptualization, Writing - review & editing. **Corinne Pau-Roblot:** Funding acquisition, Conceptualization, Writing - review & editing.

Declaration of Interest Statement:

The authors declare that they have no conflicts of interest associated with this work.

5. References:

[1] L. Hocq, S. Guinand, O. Habrylo, A. Voxeur, W. Tabi, J. Safran, F. Fournet, J.M. Domon, J.C. Mollet, S. Pilard, C. Pau-Roblot, A. Lehner, J. Pelloux, V. Lefebvre, The exogenous application of AtPGLR, an endo-polygalacturonase, triggers pollen tube burst and repair, Plant J. 103 (2020) 617–633. https://doi.org/10.1111/tpj.14753.

[2] K.H. Caffall, D. Mohnen, The structure, function, and biosynthesis of plant cell wall pectic polysaccharides, Carbohydr. Res. 344 (2009) 1879–1900. https://doi.org/10.1016/j.carres.2009.05.021.

[3] D.J. Cosgrove, Growth of the plant cell wall, Nat. Rev. Mol. Cell Biol. 6 (2005) 850–861. https://doi.org/10.1038/nrm1746.

[4] Y. Yang, Y. Yu, Y. Liang, C.T. Anderson, J. Cao, A profusion of molecular scissors for pectins: classification, expression, and functions of plant polygalacturonases, Front. Plant Sci. 9 (2018) 1–16. https://doi.org/10.3389/fpls.2018.01208.

[5] F. Sénéchal, C. Wattier, C. Rustérucci, J. Pelloux, Homogalacturonan-modifying enzymes: Structure, expression, and roles in plants, J. Exp. Bot. 65 (2014) 5125–5160. https://doi.org/10.1093/jxb/eru272.

[6] A. Kaczmarska, P.M. Pieczywek, J. Cybulska, A. Zdunek, A mini-review on the plant sources and methods for extraction of rhamnogalacturonan I, Food Chem. 403 (2023) 134378. https://doi.org/10.1016/j.foodchem.2022.134378.

[7] D. Ropartz, M.C. Ralet, Pectin structure, Pectin Technol. Physiol. Prop. (2020) 17–36. https://doi.org/10.1007/978-3-030-53421-9_2.

[8] S. Liu, L. Tian, Y. Cong, Q. Shi, L. Wang, Y. Lu, L. Wang, G. Yang, Recent advances in polygalacturonase: Industrial applications and challenges, Carbohydr. Res. 528 (2023) 108816. https://doi.org/10.1016/j.carres.2023.108816.

[9] M.A. Protsenko, N.L. Buza, A.A. Krinitsyna, E.A. Bulantseva, N.P. Korableva, Polygalacturonase-inhibiting protein is a structural component of plant cell wall, Biochem. 73 (2008) 1053–1062. https://doi.org/10.1134/S0006297908100015.

[10] C.C.V. Desagiacomo, R.C. Alnoch, V.E. Pinheiro, M. Cereia, C.B. Machado, A. Damasio, M.J. Augusto, W. Pedersoli, R.N. Silva, M. de L.T. de M. Polizeli, Structural model and functional properties of an exo-polygalacturonase from Neosartorya glabra, Int. J. Biol. Macromol. 186 (2021) 909–918.

https://doi.org/10.1016/j.ijbiomac.2021.07.065.

[11] J. Gomes, J. Zeni, K. Cence, G. Toniazzo, H. Treichel, E. Valduga, Evaluation of production and characterization of polygalacturonase by Aspergillus niger ATCC 9642, Food Bioprod. Process. 89 (2011) 281–287. https://doi.org/10.1016/j.fbp.2010.10.002.

[12] Y. Li, Y. Wang, T. Tu, D. Zhang, R. Ma, S. You, X. Wang, B. Yao, H. Luo, B. Xu, Two acidic, thermophilic GH28 polygalacturonases from Talaromyces leycettanus JCM 12802 with application potentials for grape juice clarification, Food Chem. 237 (2017) 997–1003. https://doi.org/10.1016/j.foodchem.2017.06.037.

[13] M. Kapoor, Q. Khalil Beg, B. Bhushan, K.S. Dadhich, G.S. Hoondal, Production and partial purification and characterization of a thermo-alkali stable polygalacturonase from Bacillus sp. MG-cp-2, Process Biochem. 36 (2000) 467–473. https://doi.org/10.1016/S0032-9592(00)00238-7.

[14] Y. Chen, D. Sun, Y. Zhou, L. Liu, W. Han, B. Zheng, Z. Wang, Z. Zhang, Cloning, expression and characterization of a novel thermophilic polygalacturonase from Caldicellulosiruptor bescii DSM 6725, Int. J. Mol. Sci. 15 (2014) 5717–5729. https://doi.org/10.3390/ijms15045717.

[15] J. Safran, V. Ung, J. Bouckaert, O. Habrylo, R. Molini, J. Fontaine, A. Lemaire, A. Voxeur, S. Pilard, C. Pau-roblot, S. Fabien, D. Mercadante, The specificity of pectate lyase VdPelB from Verticilium dahliae is highlighted by structural , dynamical and biochemical characterizations, Int. J. Biol. Macromol. 231 (2023) 1–12. https://doi.org/10.1016/j.ijbiomac.2023.123137.

[16] T. Ohashi, N. Sari, R. Misaki, K. Fujiyama, Biochemical characterization of Arabidopsis clade F polygalacturonase shows a substrate preference toward oligogalacturonic acids, J. Biosci. Bioeng. 133 (2022) 1–7. https://doi.org/10.1016/j.jbiosc.2021.08.007.

[17] R. Tanaka, M. Ikeda, K. Funatsuki, H. Yukioka, Y. Hashimoto, S. Fujimoto, M. Takata, K. Katoh, H. Konno, Molecular cloning and cytochemical analysis of exopolygalacturonase from carrot, Planta. 215 (2002) 735–744. https://doi.org/10.1007/s00425-002-0807-4.

[18] Enzyme market in market research, Market Research Reports, 2022.

[19] Global polygalacturonase market report : 2031 key insights in market report and

forecast, Market Research Intellect, 2024.

[20] S. Barman, N. Sit, L.S. Badwaik, S.C. Deka, Pectinase production by Aspergillus niger using banana (Musa balbisiana) peel as substrate and its effect on clarification of banana juice, J. Food Sci. Technol. 52 (2015) 3579–3589. https://doi.org/10.1007/s13197-014-1413-8.

[21] A. Roman-Benn, C.A. Contador, M.W. Li, H.M. Lam, K. Ah-Hen, P.E. Ulloa, M.C. Ravanal, Pectin: An overview of sources, extraction and applications in food products, biomedical, pharmaceutical and environmental issues, Food Chem. Adv. 2 (2023) 100192. https://doi.org/10.1016/j.focha.2023.100192.

[22] E. Karataş, A. Tülek, D. Yildirim, F. Tamtürk, B. Binay, Immobilization of Sporothrix schenckii 1099-18 exo-polygalacturonase in magnetic mesoporous silica yolk-shell spheres: Highly reusable biocatalysts for apple juice clarification, Food Biosci. 43 (2021) 101324. https://doi.org/10.1016/j.fbio.2021.101324.

[23] F. Amin, A. Mohsin, H.N. Bhatti, M. Bilal, Production, thermodynamic characterization, and fruit juice quality improvement characteristics of an Exo-polygalacturonase from Penicillium janczewskii, Biochim. Biophys. Acta - Proteins Proteomics. 1868 (2020) 140379. https://doi.org/10.1016/j.bbapap.2020.140379.

[24] P. Yuan, K. Meng, Y. Wang, H. Luo, P. Shi, H. Huang, Y. Bai, P. Yang, B. Yao, A protease-resistant exo-polygalacturonase from Klebsiella sp. Y1 with good activity and stability over a wide pH range in the digestive tract, Bioresour. Technol. 123 (2012) 171–176. https://doi.org/10.1016/j.biortech.2012.07.037.

[25] J. Safran, W. Tabi, V. Ung, A. Lemaire, O. Habrylo, J. Bouckaert, M. Rouffle, A. Voxeur, P. Pongrac, S. Bassard, R. Molinié, J. Fontaine, S. Pilard, C. Pau-roblot, E. Bonnin, D.S. Larsen, M. Morel-rouhier, J. Girardet, V. Lefebvre, F. Sénéchal, D. Mercadante, J. Pelloux, Plant polygalacturonase structures specify enzyme dynamics and processivities to fine-tune cell wall pectins, Plant Cell. (2023) 1–19.

[26] T. Tu, Z. Wang, Y. Luo, Y. Li, X. Su, Y. Wang, J. Zhang, J. Rouvinen, B. Yao, N. Hakulinen, H. Luo, Structural Insights into the Mechanisms Underlying the Kinetic Stability of GH28 Endo-Polygalacturonase, J. Agric. Food Chem. 69 (2021) 815–823. https://doi.org/10.1021/acs.jafc.0c06941.

[27] J.A. Banks, Selaginella and 400 million years of separation, Annu. Rev. Plant Biol. 60 (2009) 223–238. https://doi.org/10.1146/annurev.arplant.59.032607.092851.

[28] J.A. Banks, T. Nishiyama, M. Hasebe, J.L. Bowman, M. Gribskov, C. DePamphilis, V.A. Albert, N. Aono, T. Aoyama, B.A. Ambrose, N.W. Ashton, M.J. Axtell, E. Barker, M.S. Barker, J.L. Bennetzen, N.D. Bonawitz, C. Chapple, C. Cheng, L.G.G. Correa, M. Dacre, J. DeBarry, I. Dreyer, M. Elias, E.M. Engstrom, M. Estelle, L. Feng, C. Finet, S.K. Floyd, W.B. Frommer, T. Fujita, L. Gramzow, M. Gutensohn, J. Harholt, M. Hattori, A. Heyl, T. Hirai, Y. Hiwatashi, M. Ishikawa, M. Iwata, K.G. Karol, B. Koehler, U. Kolukisaoglu, M. Kubo, T. Kurata, S. Lalonde, K. Li, Y. Li, A. Litt, E. Lyons, G. Manning, T. Maruyama, T.P. Michael, K. Mikami, S. Miyazaki, S.I. Morinaga, TakashiMurata, B. Mueller-Roeber, D.R. Nelson, M. Obara, Y. Oguri, R.G. Olmstead, N. Onodera, B.L. Petersen, B. Pils, M. Prigge, S.A. Rensing, D.M. Riaño-Pachón, A.W. Roberts, Y. Sato, H.V. Scheller, B. Schulz, C. Schulz, E. V. Shakirov, N. Shibagaki, N. Shinohara, D.E. Shippen, I. Sørensen, R. Sotooka, N. Sugimoto, M. Sugita, N. Sumikawa, M. Tanurdzic, G. Theißen, P. Ulvskov, S. Wakazuki, J.K. Weng, W.W.G.T. Willats, D. Wipf, P.G. Wolf, L. Yang, A.D. Zimmer, Q. Zhu, T. Mitros, U. Hellsten, D. Loqué, R. Otillar, A. Salamov, J. Schmutz, H. Shapiro, E. Lindquist, S. Lucas, D. Rokhsar, I. V. Grigoriev, The selaginella genome identifies genetic changes associated with the evolution of vascular plants, Science (80-.). 332 (2011) 960–963. https://doi.org/10.1126/science.1203810.

[29] X.M. Zhou, J. Zhao, J.J. Yang, T. Le Péchon, L. Zhang, Z.R. He, L.B. Zhang, Plastome structure, evolution, and phylogeny of Selaginella, Mol. Phylogenet. Evol. 169 (2022). https://doi.org/10.1016/j.ympev.2022.107410.

[30] H. Motte, T. Fang, B. Parizot, W. Smet, X. Yang, W. Poelmans, L. Walker, M. Njo, G.W. Bassel, T. Beeckman, Cellular and gene expression patterns associated with root bifurcation in Selaginella, Plant Physiol. 190 (2022) 2398–2416. https://doi.org/10.1093/plphys/kiac402.

[31] A. Lemaire, C. Duran Garzon, A. Perrin, O. Habrylo, P. Trezel, S. Bassard, V. Lefebvre, O. Van Wuytswinkel, A. Guillaume, C. Pau-Roblot, J. Pelloux, Three novel rhamnogalacturonan I- pectins degrading enzymes from Aspergillus aculeatinus: Biochemical characterization and application potential, Carbohydr. Polym. 248 (2020) 116752. https://doi.org/10.1016/j.carbpol.2020.116752.

[32] T.C. McIlvaine, a Buffer Solution for Colorimetric Comparison, J. Biol. Chem. 49 (1921) 183–186. https://doi.org/10.1016/s0021-9258(18)86000-8.

[33] G.L. Miller, Use of Dinitrosalicylic Acid Reagent for Determination of Reducing Sugar, Anal. Chem. 31 (1959) 426–428. https://doi.org/10.1021/ac60147a030.

[34] S. Forli, R. Huey, M.E. Pique, M.F. Sanner, D.S. Goodsell, A.J. Olson, Computational protein–ligand docking and virtual drug screening with the AutoDock suite, Nat. Protoc. 11 (2016) 905–919. https://doi.org/10.1038/nprot.2016.051.

[35] E.F. Pettersen, T.D. Goddard, C.C. Huang, G.S. Couch, D.M. Greenblatt, E.C. Meng, T.E. Ferrin, UCSF Chimera--A visualization system for exploratory research and analysis, J. Comput. Chem. 25 (2004) 1605–1612. https://doi.org/10.1002/jcc.20084.

[36] M.J. Abraham, T. Murtola, R. Schulz, S. Páll, J.C. Smith, B. Hess, E. Lindah, Gromacs: High performance molecular simulations through multi-level parallelism from laptops to supercomputers, SoftwareX. 1–2 (2015) 19–25. https://doi.org/10.1016/j.softx.2015.06.001.

[37] J. Huang, S. Rauscher, G. Nawrocki, T. Ran, M. Feig, B.L. De Groot, H. Grubmüller, A.D. MacKerell, CHARMM36m: An improved force field for folded and intrinsically disordered proteins, Nat. Methods. 14 (2016) 71–73. https://doi.org/10.1038/nmeth.4067.

[38] J. Lee, X. Cheng, J.M. Swails, M.S. Yeom, P.K. Eastman, J.A. Lemkul, S. Wei, J. Buckner, J.C. Jeong, Y. Qi, S. Jo, V.S. Pande, D.A. Case, C.L. Brooks, A.D. MacKerell, J.B. Klauda, W. Im, CHARMM-GUI Input Generator for NAMD, GROMACS, AMBER, OpenMM, and CHARMM/OpenMM Simulations Using the CHARMM36 Additive Force Field, J. Chem. Theory Comput. 12 (2016) 405–413. https://doi.org/10.1021/acs.jctc.5b00935.

[39] S. Kim, J. Lee, S. Jo, C.L. Brooks, H.S. Lee, W. Im, CHARMM-GUI ligand reader and modeler for CHARMM force field generation of small molecules, J. Comput. Chem. 38 (2017) 1879–1886. https://doi.org/10.1002/jcc.24829.

[40] J. Wang, W. Wang, P. a Kollman, D. a Case, Antechamber, An Accessory Software Package For Molecular Mechanical Calculations, J. Am. Chem. Soc. 222 (2001) U403.

[41] D.A. Case, R.C. Walker, T.E. Cheatham III, C. Simmerling, A. Roitberg, K.M. Merz, R. Luo, P. Li, T. Darden, C. Sagui, F. Pan, J. Wang, D.R. Roe, S. LeGrand, J. Swails, A.W. Götz, J. Smith, D. Cerutti, T. Lee, D. York, T. Luchko, V. Man, V.W.D. Cruzeiro, G. Monard, Y. Miao, J. Wang, R.M. Wolf, C. Lin, G.A. Cisneros, A. Rahnamoun, A. Shajan, M. Manathunga, J.T. Berryman, R.E. Duke, N.R. Skrynnikov, O. Mikhailovskii, Y. Xue, S.A. Izmailov, K. Kasavajhala, K. Belfon, J. Shen, R. Harris, A. Onufriev, S. Izadi, Y. Xiong, X. Wu, H. Gohlke, S. Schott-Verdugo, R. Qi, H. Wei, S. Zhao, E. King,

G. Giambasu, J. Liu, H. Nguyen, S.R. Brozell, A. Kovalenko, M. Gilson, I. Ben-Shalom, T. Kurtzman, S. Pantano, M. Machado, H.M. Aktulga, M.C. Kaymak, K.A. O'Hearn, P.A. Kollman, Amber 2022 Reference Manual Principal contributors to the current codes, (2022) 0–1013. https://ambermd.org/contributors.html.

[42] J.B.H.J.C.P.J.P.M. van G.W.F. Hermans, Interaction Models for Water in Relation to Protein Hydration, in: Jerusalem Symp. Quantum Chem. Biochem., 1981: pp. 331–342. https://doi.org/10.1007/978-94-015-7658-1_21.

[43] M. Parrinello, A. Rahman, Polymorphic transitions in single crystals: A new molecular dynamics method, J. Appl. Phys. 52 (1981) 7182–7190. https://doi.org/10.1063/1.328693.

[44] S. Nosé, A unified formulation of the constant temperature molecular dynamics methods, J. Chem. Phys. 81 (1984) 511–519. https://doi.org/10.1063/1.447334.

[45] W.G. Hoover, Canonical Dynamics: Equilibrium Phase-Space Distributions, Gen. Phys. 931 (1985) 1695–97. https://doi.org/10.1103/PhysRevA.31.1695.

[46] B. Hess, P-LINCS: A parallel linear constraint solver for molecular simulation, J. Chem. Theory Comput. 4 (2008) 116–122. https://doi.org/10.1021/ct700200b.

[47] F. Ramos-Martín, C. Herrera-León, V. Antonietti, P. Sonnet, C. Sarazin, N. D'amelio, Antimicrobial peptide k11 selectively recognizes bacterial biomimetic membranes and acts by twisting their bilayers, Pharmaceuticals. 14 (2021) 1–22. https://doi.org/10.3390/ph14010001.

[48] W. Humphrey, A. Dalke, K. Schulten, VMD - Visual Molecular Dynamics, J. Mol. Graph. 14 (1996) 33–38.

[49] A. Voxeur, O. Habrylo, S. Guénin, F. Miart, M.C. Soulié, C. Rihouey, C. Pau-Roblot, J.M. Domon, L. Gutierrez, J. Pelloux, G. Mouille, M. Fagard, H. Höfte, S. Vernhettes, Oligogalacturonide production upon Arabidopsis thaliana-Botrytis cinerea interaction, Proc. Natl. Acad. Sci. U. S. A. 116 (2019) 19743–19752. https://doi.org/10.1073/pnas.1900317116.

[50] D.E. Evangelista, E.A. de Araújo, M.O. Neto, M.A.S. Kadowaki, I. Polikarpov, Biochemical characterization and low-resolution SAXS structure of an exo-polygalacturonase from Bacillus licheniformis, N. Biotechnol. 40 (2018) 268–274. https://doi.org/10.1016/j.nbt.2017.10.001.

[51] D.W. Abbott, A.B. Boraston, The Structural Basis for Exopolygalacturonase Activity in a Family 28 Glycoside Hydrolase, J. Mol. Biol. 368 (2007) 1215–1222. https://doi.org/10.1016/j.jmb.2007.02.083.

[52] S.W. Cho, S. Lee, W. Shin, The X-ray structure of Aspergillus aculeatus polygalacturonase and a modeled structure of the polygalacturonase-octagalacturonate complex, J. Mol. Biol. 311 (2001) 863–878. https://doi.org/10.1006/jmbi.2001.4919.

[53] S. Proost, M. Mutwil, CoNekT: An open-source framework for comparative genomic and transcriptomic network analyses, Nucleic Acids Res. 46 (2018) W133–W140. https://doi.org/10.1093/nar/gky336.

[54] C. Ferrari, D. Shivhare, B.O. Hansen, A. Pasha, E. Esteban, N.J. Provart, F. Kragler, A. Fernie, T. Tohge, M. Mutwil, Expression atlas of selaginella moellendorffii provides insights into the evolution of vasculature, secondary metabolism, and roots, Plant Cell. 32 (2020) 853–870. https://doi.org/10.1105/TPC.19.00780.

[55] J. Safran, O. Habrylo, M. Cherkaoui, S. Lecomte, A. Voxeur, S. Pilard, S. Bassard, C. Pau-Roblot, D. Mercadante, J. Pelloux, F. Sénéchal, New insights into the specificity and processivity of two novel pectinases from Verticillium dahliae, Int. J. Biol. Macromol. 176 (2021) 165–176. https://doi.org/10.1016/j.ijbiomac.2021.02.035.

[56] N.A. Devi, A.G.A. Rao, fungus Aspergillus Purification of PG II, 44 (1998) 79–87.

[57] X. Ma, W. Wang, M. Zou, T. Ding, X. Ye, D. Liu, Properties and structures of commercial polygalacturonase with ultrasound treatment: Role of ultrasound in enzyme activation, RSC Adv. 5 (2015) 107591–107600. https://doi.org/10.1039/c5ra19425c.

[58] V. Poondla, R. Chikati, M. Kallubai, Characterization and molecular modeling of polygalacturonase isoforms from Saccharomyces cerevisiae, 3 Biotech. 7 (2017) 1–13. https://doi.org/10.1007/s13205-017-0912-5.

[59] Y. Liu, W. Qu, Y. Liu, J.A. Tuly, H. Ma, MD simulation to comprehend polygalacturonase inactivation mechanism during thermal and non-thermal effects of infrared processing, Food Chem. 441 (2023) 138298. https://doi.org/10.1016/j.foodchem.2023.138298.

[60] Z. Cheng, D. Chen, B. Lu, Y. Wei, L. Xian, Y. Li, Z. Luo, R. Huang, A Novel acid-stable

endo-polygalacturonase from Penicillium oxalicum CZ1028: Purification, characterization, and application in the beverage industry, J. Microbiol. Biotechnol. 26 (2016) 989–998. https://doi.org/10.4014/jmb.1511.11045.

[61] O. Habrylo, D.E. Evangelista, P.V. Castilho, J. Pelloux, F. Henrique-Silva, The pectinases from Sphenophorus levis: Potential for biotechnological applications, Int. J. Biol. Macromol. 112 (2018) 499–508. https://doi.org/10.1016/j.ijbiomac.2018.01.172.

[62] H.T. Chan, S.Y.. Tam, Partial Separation and Characterization of Papaya Endo- and Exo-Polygalacturonase, J. Food Sci. 47 (1982) 1478–1483. https://doi.org/https://doi.org/10.1111/j.1365-2621.1982.tb04965.x.

[63] L. Hocq, J. Pelloux, V. Lefebvre, Connecting Homogalacturonan-Type Pectin Remodeling to Acid Growth, Trends Plant Sci. 22 (2017) 20–29. https://doi.org/10.1016/j.tplants.2016.10.009.

[64] H. Doostdar, T.G. McCollum, R.T. Mayer, Purification and characterization of an endo-polygalacturonase from the gut of west indies sugarcane rootstalk borer weevil (Diaprepes abbreviatus L.) Larvae, Comp. Biochem. Physiol. - B Biochem. Mol. Biol. 118 (1997) 861–867. https://doi.org/10.1016/S0305-0491(97)00285-X.

[65] S. Ullah, A.S. Khan, A.U. Malik, M. Shahid, K. Razzaq, Cultivar, harvest location and cold storage influence fruit softening and antioxidative activities of peach fruit [Prunus persica (L.) Batsch.], Pakistan J. Bot. 47 (2015) 699–709.

[66] M.D.L.P. Celorio-Mancera, L.C. Greve, L.R. Teuber, J.M. Labavitch, Identification of endo- and exo-polygalacturonase activity in Lygus hesperus (Knight) salivary glands, Arch. Insect Biochem. Physiol. 70 (2009) 122–135. https://doi.org/10.1002/arch.20282.

[67] G.A. Morris, J. Castile, A. Smith, G.G. Adams, S.E. Harding, The effect of different storage temperatures on the physical properties of pectin solutions and gels, Polym. Degrad. Stab. 95 (2010) 2670–2673. https://doi.org/10.1016/j.polymdegradstab.2010.07.013.

[68] A. Thakur, R. Pahwa, S. Singh, R. Gupta, Production, purification, and characterization of polygalacturonase from mucor circinelloides ITCC 6025, Enzyme Res. 2010 (2010). https://doi.org/10.4061/2010/170549.

[69] M. L'Enfant, J.M. Domon, C. Rayon, T. Desnos, M.C. Ralet, E. Bonnin, J. Pelloux, C. Pau-Roblot, Substrate specificity of plant and fungi pectin methylesterases:

Identification of novel inhibitors of PMEs, Int. J. Biol. Macromol. 81 (2015) 681–691. https://doi.org/10.1016/j.ijbiomac.2015.08.066.

[70] K.C. Lewis, T. Selzer, C. Shahar, Y. Udi, D. Tworowski, I. Sagi, Inhibition of pectin methyl esterase activity by green tea catechins, Phytochemistry. 69 (2008) 2586–2592. https://doi.org/10.1016/j.phytochem.2008.08.012.

[71] S. Nakano, S. Megro, T. Hase, T. Suzuki, M. Isemura, Y. Nakamura, S. Ito, Computational Molecular Docking and X-ray Crystallographic Studies of Catechins in New Drug Design Strategies, Molecules. 23 (2018) 1–28. https://doi.org/10.3390/molecules23082020.

[72] F. Xu, M. Gonneau, E. Faucher, O. Habrylo, V. Lefebvre, J.M. Domon, M. Martin, F. Sénéchal, A. Peaucelle, J. Pelloux, H. Höfte, Biochemical characterization of Pectin Methylesterase Inhibitor 3 from Arabidopsis thaliana, Cell Surf. 8 (2022) 4–11. https://doi.org/10.1016/j.tcsw.2022.100080.

Highlights:

SmoPG1 is most expressed in shoots where it shows importance in development.
SmoPG1 is the first produced and characterized exo-polygalacturonase in *S. moellendorffii*.
Docking studies and MD simulation highlight EGCG inhibition of pectinases.

Table 1. Effect of metals ions on SmoPG1 activity. The activity was measured by DNS test with SmoPG1 and PGA at 0.4 % final in McIlvain buffer at pH 5 during 30 min.

Ions (1mM)	Relative activity (%)
Control	100 ± 7.9
Ca^{2+}	46.0 ± 4.7
Cu^{2+}	123.0 ± 2.7
Fe^{2+}	68.1 ± 2.6
Mg^{2+}	129.2 ± 0.0
Mn^{2+}	133.6 ± 2.7
Na^{2+}	146.9 ± 3.5
Zn^{2+}	168.1 ± 5.9

Table 2. Docking studies reveal amino acids of SmoPG1 involved in interaction with EGCG. For each repetition three docked EGCG with highest affinity were selected and the H-bond interaction were studied.

Repetition	1			2			3			4		
Rank	1	2	3	1	2	3	1	2	3	1	2	3
Binding energy (kcal/mol)	-7,3	-7,0	-6,7	-7,6	-7,5	-6,8	-7,6	-7,5	-7,2	-6,7	-6,6	-5,4
H-bonds interactions	D234	N237	D260	R139	R139	R139	D362	R139	E140	W212	W212	N237
	N237	K266	K322	W212	N237	E140	E140	R326	N237	D239	N237	S295
	D260	S295	R323	N237	D261	D237	N237	Y360	G259	V294	G259	R323
	K322	R326	-	G259	S295	D362	R139	D362	Y360	S295	K266	R326
	R323	-	-	E303	E303	-	-	-	-	R326	K328	-
	Y360	-	-	R326	R326	-	-	-	-	-	-	-
	-	-	-	D362	Y360	-	-	-	-	-	-	-

Figures captions:

Fig.1. Phylogenetic analysis and modelisation with Alphafold model of SmoPG1 indicating is a potential exo-PG.

(**A**) Phylogenetic tree representing *S. moellendorffii (*SmoPG1) amino acid sequence in comparison with PGs from *Selaginella moellendorffii:* Uniprot accession and nomenclature numbers of the SmoPGs are presented, *Arabidopsis thaliana:* AtPGF10 (Q9FPJ2), AtPGF7 (A0A384LBD5), AtPGF12 (A0A5S9XVT1), AtPGLR (Q9LYJ5), AtADPG2 (Q8RY29)), *Yersinia enterocolitica:* YePG (O68975) and *Bacillus licheniformis*: BlPG (Q65F26). (**B**) Modelisation of SmoPG1: Alphafold model of SmoPG1 indicating conserved β-helical structure. (**C**) Superposition of SmoPG1 model with AtPGF10 (43 % identity, green) and YePG (24% identity, gold) shown to be exo-PGs. (**D**) Active site residue of SmoPG1 (pink), AtPGF10 (green) and YePG (gold).

Fig. 2. *S. moellendorffii* transcriptomic analysis.

(**A**) Heat map genes expression in *S. moellendorffii* tissus (Ferrari et al., 2020) (**B**) Image highlighting *S. moellendorffii* roots and shoot morphology during development. (**C**) Violin plot highlighting SmoPG1 expression levels in roots and shoots. Data represent average ± SD; n = 3. Multiple one way anova's with tukey's multiple comparison test was realized α=0.05.
* P<0.05 and ** P<0.01

Fig. 3. SmoPG1 production, biochemical characterization and oligoprofiling show that SmoPG1 is an exo-PG

(A) SmoPG1 was purified by affinity chromatography after its expression in *Pichia pastoris*. Purified protein was denatured and incubated for 60 min at 37 °C in the presence (lane 1) or absence (lane 2) of peptide-N- glycosidase F (PNGase). Samples were loaded for SDS-PAGE and stained with Coomassie blue. L, molecular weight markers. **(B)** SmoPG1 circular dichroism spectra and CD Multivariate Secondary Structure Estimation: The secondary structure was determined by CD Multivariate Secondary Structure Estimation (SSE) program (Jasco), using the principal components regression (PCR) and partial least square (PLS) multivariate method. **(C)** Effect of different substrates on SmoPG1 activity. Reactions were carried out at 50 °C for 120 min using substrates (0.4 % final) with different pattern of methyl-esterification and acetylation: polygalacturonic acid (PGA), citrus pectins (DM 55 to 70 %, DM 71 %), sugar beet pectin (DM 42 %, DA 31 %) and apple pectin (DM 70 to 75 %). The PG activity was measured by DNS method at pH 5. Data represent average ± SD; n = 3. **(D)** Influence of the temperature on SmoPG1 activity by determination of optimal temperature (black line) and thermostability (grey line). The activity was measured by DNS test with SmoPG1 and PGA at 0.4 % final at pH 5 during 30 min between 25 to 60 °C. Data represent average ± SD; n = 3. **(E)** Influence of the pH on SmoPG1 activity by determination of optimal

pH (black line) and pH stability (grey line). The activity was measured by DNS test with SmoPG1 and PGA at 0.4 % final at pH 4 to 8 during 30 min. Data represent average ± SD; n = 3. **(F)** Determination of kinetic constants of SmoPG1. Activity was assessed using various concentrations of PGA at 50°C and pH 5. Data represent average ± SD; n = 3. **(G)** Analysis of OGs released by SmoPG1 from PGA incubated 2 h, and O/N. Data are means ± SD; n = 3. Subscript numbers indicate the DP and DM. Data represent average ± SD; n = 3. **(H)** Analysis of OGs released by SmoPG1 from citrus pectins DM55-70% incubated 2 h and O/N. Data represent average ± SD; n = 3.

Fig. 4. Effect of inhibitors on SmoPG1 activity and docking studies highlight EGCG and SmoPG1 interactions.

(A) The activity of SmoPG1 was measured by DNS test with tannic acid (0,02 mg/mL and 0.002 mg/mL), EGCG (0.5mg/mL), PP60 (1.25mg/mL) and without inhibitors. **(B)** The effect of EGCG was studding by docking showing EGCG (dark cyan) to SmoPG1 (pink) model. **(C)** Detailed presentation of EGCG (dark cyan) H-bond interactions with SmoPG1 (pink) amino acids (green).

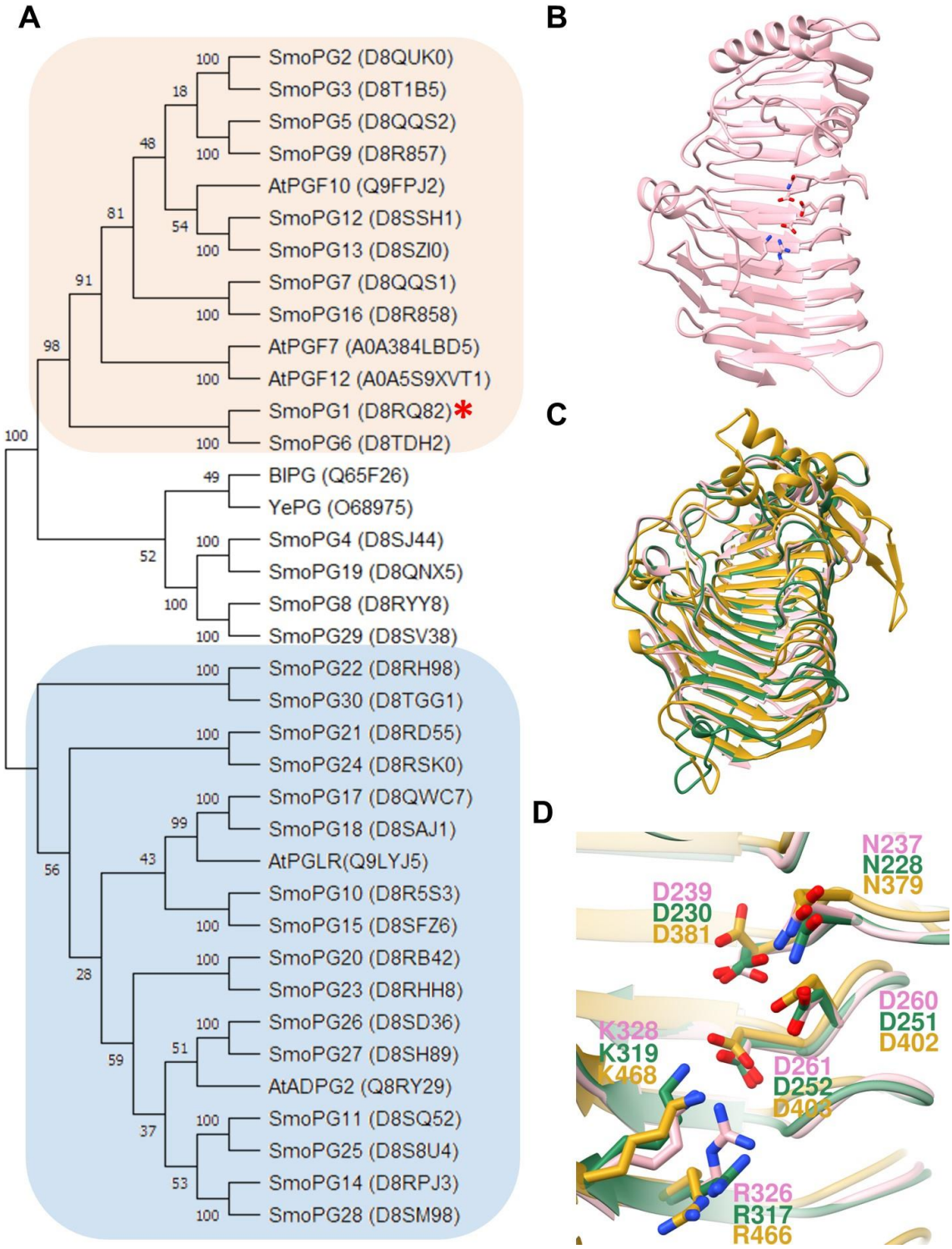
A
SmoPG2 (D8QUK0)
SmoPG3 (D8T1B5)
SmoPG5 (D8QQS2)
SmoPG9 (D8R857)
AtPGF10 (Q9FPJ2)
SmoPG12 (D8SSH1)
SmoPG13 (D8SZI0)
SmoPG7 (D8QQS1)
SmoPG16 (D8R858)
AtPGF7 (A0A384LBD5)
AtPGF12 (A0A5S9XVT1)
SmoPG1 (D8RQ82)*
SmoPG6 (D8TDH2)
BIPG (Q65F26)
YePG (O68975)
SmoPG4 (D8SJ44)
SmoPG19 (D8QNX5)
SmoPG8 (D8RYY8)
SmoPG29 (D8SV38)
SmoPG22 (D8RH98)
SmoPG30 (D8TGG1)
SmoPG21 (D8RD55)
SmoPG24 (D8RSK0)
SmoPG17 (D8QWC7)
SmoPG18 (D8SAJ1)
AtPGLR(Q9LYJ5)
SmoPG10 (D8R5S3)
SmoPG15 (D8SFZ6)
SmoPG20 (D8RB42)
SmoPG23 (D8RHH8)
SmoPG26 (D8SD36)
SmoPG27 (D8SH89)
AtADPG2 (Q8RY29)
SmoPG11 (D8SQ52)
SmoPG25 (D8S8U4)
SmoPG14 (D8RPJ3)
SmoPG28 (D8SM98)
B
C
D
N237
N228
N379
D239
D230
D381
D260
D251
D402
K328
K319
K468
D261
D252
D403
R326
R317
R466

Figure 1

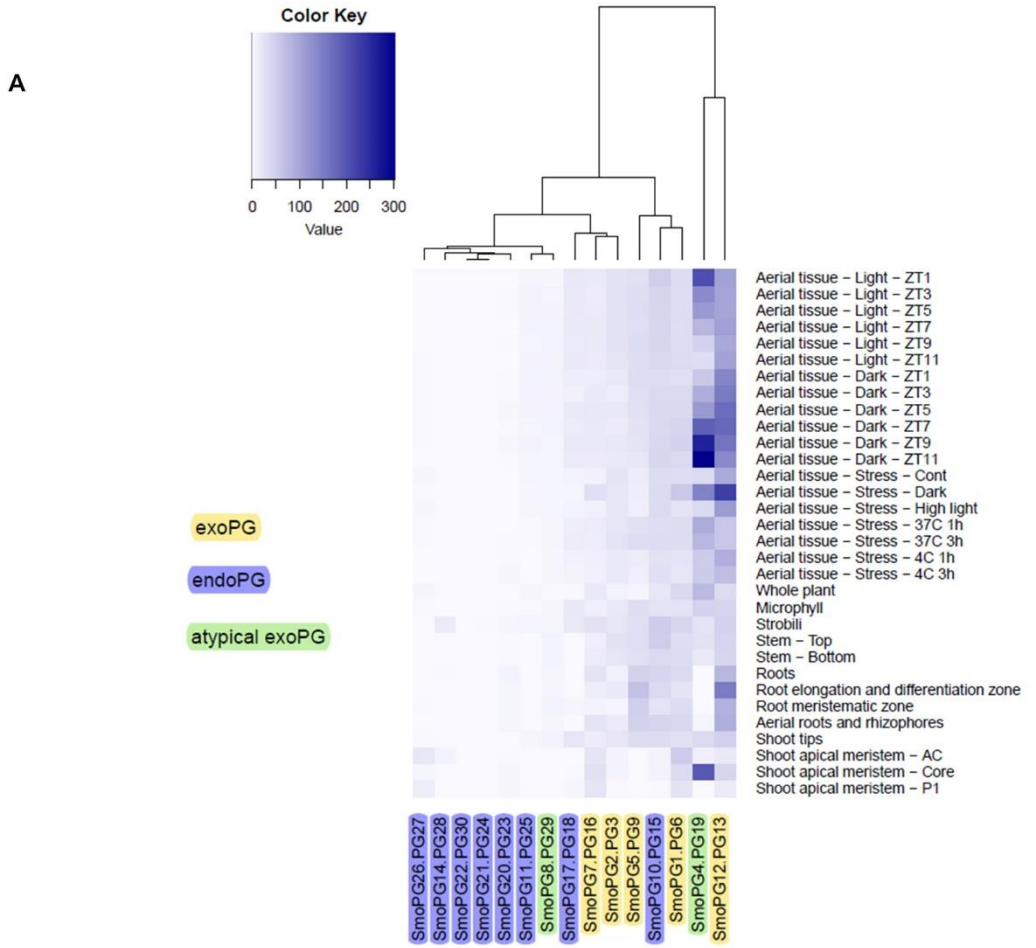

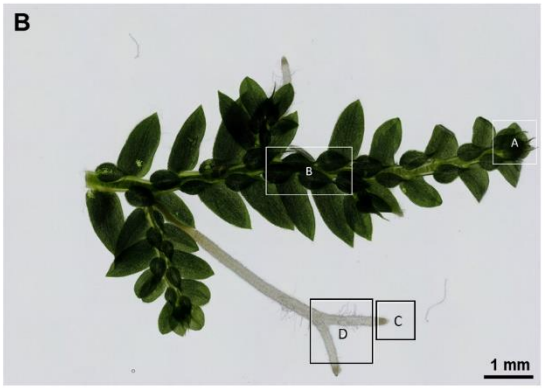

A : Shoot tip B : Shoot segment
C : Root tip D : Root segment

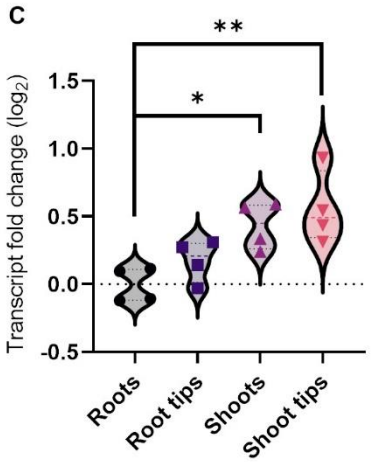

Figure 2

A

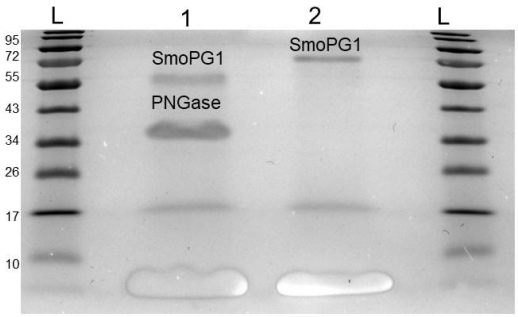

B

SSE method	T (°C)	α-helix (%)	β-sheet (%)	Turn (%)	Other (%)
PCR	20	12	30.1	13.2	44.7
	45	3.5	40.5	15.9	40.1
	60	6.5	38.8	15.7	39
PLS	20	14.7	29.7	11.4	44.2
	45	4.5	36.3	19.9	39.3
	60	8.4	34.2	18.7	38.7

C

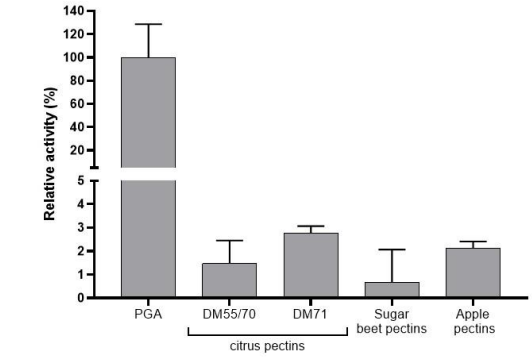

D

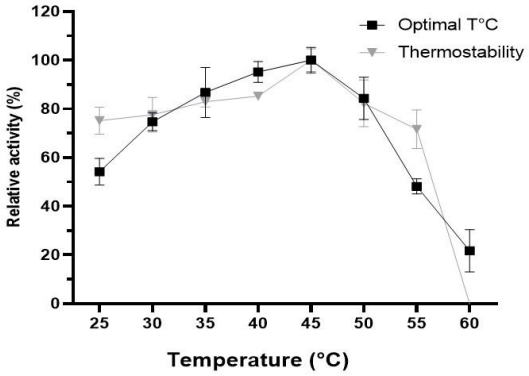

E

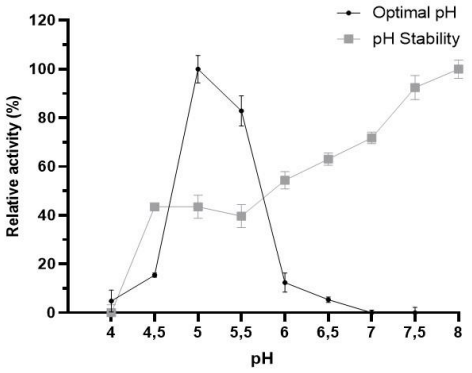

F

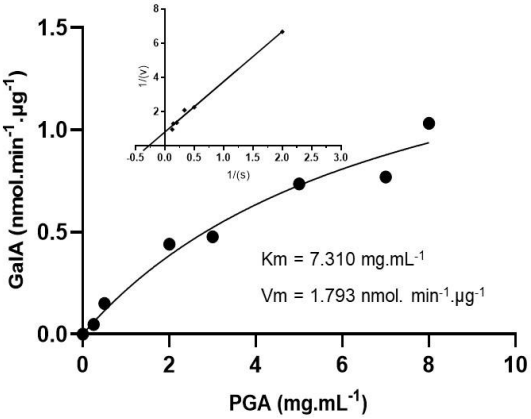

G

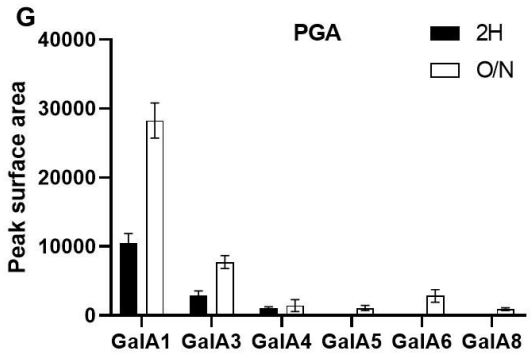

H

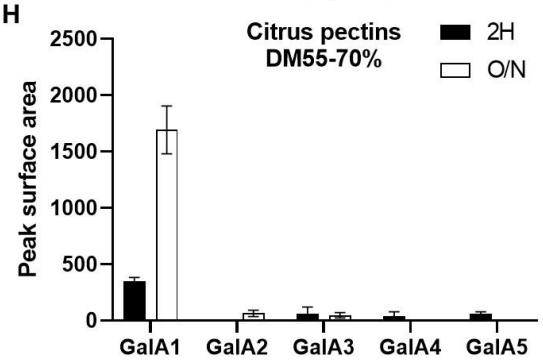

Figure 3

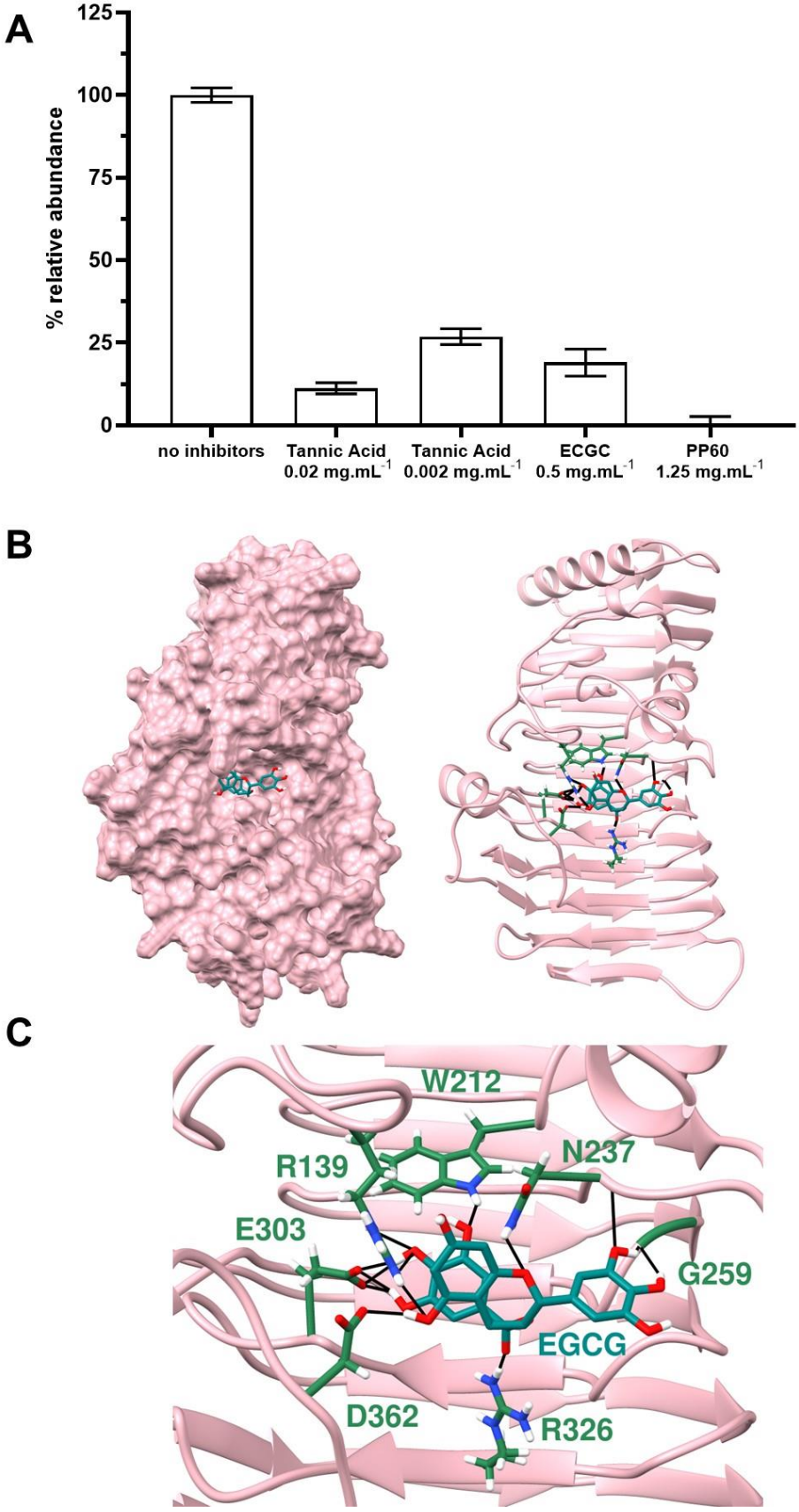
A
125
100
75
50
25
0
% relative abundance
no inhibitors
Tannic Acid 0.02 mg.mL-1
Tannic Acid 0.002 mg.mL-1
ECGC 0.5 mg.mL-1
PP60 1.25 mg.mL-1
B
C
W212
N237
R139
E303
G259
EGCG
D362
R326

Figure 4

Supplementary Table S1. Analyse of sequences identities of *S. moellendorffii* polygalacturonase 1 (SmoPG1) with selected polygalacturonases. Table includes PGs from *Selaginella moellendorffii :* SmoPG1 (uniport : D8RQ82), SmoPG2 (D8QUK0),SmoPG3 (D8T1B5), SmoPG4 (D8SJ44), SmoPG5 (D8QQS2), SmoPG6 (D8TDH2), SmoPG7 (D8QQS21), DmoPG8 (D8RYY8), SmoPG9 (D8R857), SmoPG10 (D8R5S3), SmoPG11 (D8SQ52), SmoPG12 (D8SSH1), SmoPG13 (D8SZI0), SmoPG14 (D8RPJ3), SmoPG15 (D8SFZ6), SmoPG16 (D8R858), SmoPG17 (D8QWC7), SmoPG18 (D8SAJ1), SmoPG19 (D8QNX5), SmoPG20 (D8RB42), SmoPG21 (D8RD55), SmoPG23 (D8RHH8), SmoPG24 (D8RQK0), SmoPG25 (D8S8U4), SmoPG26 (D8SD36), SmoPG27 (D8SH89), SmoPG28 (D8SM98), SmoPG29 (D8SV38), SmoPG30 (D8TGG1), *Arabidopsis thaliana :* AtPGF10 (Q9FPJ2), AtPGF7 (A0A384LBD5), AtPGF12 (A0A5S9XVT1), AtPGLR (Q9LYJ5), AtADPG2 (Q8RY29)) and *Yersinia enterocolitica :* YePG (O68975) and *Bacillus licheniformis* : BlPG (Q65F26). **Blue: high sequence identity**; **Red: low sequence identity.**

	SmoPG22	SmoPG30	SmoPG26	SmoPG27	AtPGLR	SmoPG17	SmoPG18	SmoPG21	SmoPG24	AtADPG2	SmoPG10	SmoPG15	SmoPG14	SmoPG28	SmoPG11	SmoPG25	SmoPG20	SmoPG23	SmoPG8	SmoPG29	SmoPG4	SmoPG19	YePG	BlPG	SmoPG1	SmoPG6	AtPGF7	AtPGF12	SmoPG7	SmoPG16	SmoPG2	SmoPG3	SmoPG5	SmoPG9	AtPGF10	SmoPG12	SmoPG13
SmoPG22	100	98,5	40,54	40,54	38,1	40,53	40,64	43,39	43,1	39,19	39,42	39,42	40,06	40,57	39,82	39,82	45,91	44,97	20,43	20,12	20,81	20,68	18,41	21,5	27,41	27,11	26,41	24,72	26,38	27,55	26,17	25,86	27,2	27,2	29,08	26,89	26,59
SmoPG30	98,5	100	41,78	41,78	37,93	40,91	41,01	42,51	42,51	39,04	39,62	39,62	39,26	39,71	38,36	38,36	45,06	43,9	20,06	20,34	20,4	20,29	17,97	22,16	26,5	26,23	26,46	24,61	25,89	26,96	25,22	24,93	26,13	26,13	28,69	26,06	25,78
SmoPG26	40,54	41,78	100	97,62	38,93	38,16	37,96	38,44	38,44	43,88	39,43	39,43	42,71	42,44	40,32	40,32	41,24	40,97	19,72	19,72	18,28	18,46	21,68	23,23	23,64	23,91	22,44	23,08	21,64	21,85	23,06	23,33	23,33	23,33	27,12	25,35	25,07
SmoPG27	40,54	41,78	97,62	100	38,67	38,16	37,8	38,18	38,18	43,62	39,16	39,16	42,44	42,18	40,05	40,05	40,7	40,43	19,72	19,72	18,56	18,73	21,14	22,66	23,91	24,18	22,16	22,8	21,64	21,85	23,06	23,33	23,61	23,61	26,85	24,79	24,51
AtPGLR	38,1	37,93	38,93	38,67	100	51,29	51,17	40,3	39,8	41,5	43,36	43,61	41,62	41,62	36,43	36,43	41,3	41,3	22,25	21,98	21,07	21,75	18,43	22,51	26,41	26,41	24,08	24,1	20	20,88	25,34	25,07	23,26	23,2	25,46	22,46	22,73
SmoPG17	40,53	40,91	38,16	38,16	51,29	100	98,9	37,8	37,8	39,13	41,56	42,05	39,84	40	39,29	39,04	41,98	41,18	17,4	17,92	19,06	19,22	19,31	21,33	26,65	26,9	21,77	21,8	21,34	22,28	24,8	24,8	24,22	24,42	25,71	23,02	22,75
SmoPG18	40,64	41,01	37,96	37,8	51,17	98,9	100	38,05	38,05	38,74	41,32	41,81	39,31	39,47	39,04	38,79	41,71	40,91	17,14	17,66	18,8	18,96	19,06	21,33	26,4	26,65	21,77	21,8	21,34	22,01	24,53	24,53	23,7	23,9	25,45	23,02	22,75
SmoPG21	43,39	42,51	38,44	38,18	40,3	37,8	38,05	100	97,93	41,27	40,44	40,2	38,8	38,95	37,37	37,37	43,2	43,2	20,36	19,85	18,97	18,62	19,02	20,56	25,7	25,45	23,51	22,34	21,5	22,1	23,53	22,99	22,11	22,05	25,9	22,43	22,69
SmoPG24	43,1	42,51	38,44	38,18	39,8	37,8	38,05	97,93	100	41,52	40,44	40,2	38,8	38,95	37,88	37,88	42,67	42,67	20,36	19,85	18,97	18,62	19,02	20,56	25,45	25,19	23,26	22,08	21,5	22,1	23,8	23,26	22,11	22,05	25,9	22,43	22,69
AtADPG2	39,19	39,04	43,88	43,62	41,5	39,13	38,74	41,27	41,52	100	42,39	42,39	42,93	43,4	43,41	43,41	43,94	43,67	21,15	22,25	19,83	20,55	22,89	24,72	27,06	26,79	27,3	24,54	23,48	24,03	26,74	26,74	25,46	25,46	27,57	26,92	26,65
SmoPG10	39,42	39,62	39,43	39,16	43,36	41,56	41,32	40,44	40,44	42,39	100	97,61	42,97	43,04	40,3	40,3	42,97	43,5	18,01	18,01	20,33	20,49	19,21	19,22	25,13	25,13	21,64	25,07	22,02	22,01	25,2	25,2	21,87	21,81	25,07	22,02	22,28
SmoPG15	39,42	39,62	39,43	39,16	43,61	42,05	41,81	40,2	40,2	42,39	97,61	100	42,97	43,04	40,8	40,8	42,44	42,97	18,01	18,01	20,6	20,75	19,47	19,5	25,39	25,39	21,9	25,33	22,28	22,28	25,75	25,75	21,87	21,81	25,07	22,28	22,55
SmoPG14	40,06	39,26	42,71	42,44	41,62	39,84	39,31	38,8	38,8	42,93	42,97	42,97	100	99,48	44,7	44,7	42,86	43,12	18,98	18,7	19,27	19,55	20,33	21,65	25,56	25,56	23,96	24,79	26,26	26,26	26,11	26,11	25,49	25,49	25,35	23,96	23,68
SmoPG28	40,57	39,71	42,44	42,18	41,62	40	39,47	38,95	38,95	43,4	43,04	43,04	99,48	100	44,91	44,91	43,09	43,35	19,32	19,03	19,33	19,61	20,39	21,71	25,63	25,63	24,02	24,58	26,61	26,61	26,18	26,18	25,56	25,56	25,14	24,02	23,74
SmoPG11	39,82	38,36	40,32	40,05	36,43	39,29	39,04	37,37	37,88	43,41	40,3	40,8	44,7	44,91	100	99,51	44,62	44,88	20,33	20,6	20	20,22	21,75	23,2	29,33	29,07	22,93	25,99	26,88	27,03	29,08	29,08	27,01	27,01	27,27	26,93	26,67
SmoPG25	39,82	38,36	40,32	40,05	36,43	39,04	38,79	37,37	37,88	43,41	40,3	40,8	44,7	44,91	99,51	100	44,62	44,88	20,33	20,6	20	20,22	21,75	23,2	29,33	29,07	22,93	25,99	26,88	27,03	29,08	29,08	27,01	27,01	27,27	26,93	26,67
SmoPG20	45,91	45,06	41,24	40,7	41,3	41,98	41,71	43,2	42,67	43,94	42,97	42,44	42,86	43,09	44,62	44,62	100	97,65	20,46	20,17	21,43	22	20,73	23,65	29,94	29,66	25,71	23,73	26,14	26,14	27,48	27,48	26,78	26,78	28,81	27,68	27,97
SmoPG23	44,97	43,9	40,97	40,43	41,3	41,18	40,91	43,2	42,67	43,67	43,5	42,97	43,12	43,35	44,88	44,88	97,65	100	21,04	20,75	21,71	22,29	21,01	24,22	29,94	29,66	24,86	23,73	26,42	26,42	28,05	28,05	26,78	26,78	29,1	27,12	27,4
SmoPG8	20,43	20,06	19,72	19,72	22,25	17,4	17,14	20,36	20,36	21,15	18,01	18,01	18,98	19,32	20,33	20,33	20,46	21,04	100	98,29	50,55	50,87	25,69	22,74	23,31	22,81	23,84	23,32	24,87	25,54	25,07	24,8	25,19	25,19	24,38	23,14	23,14
SmoPG29	20,12	20,34	19,72	19,72	21,98	17,92	17,66	19,85	19,85	22,25	18,01	18,01	18,7	19,03	20,6	20,6	20,17	20,75	98,29	100	50,55	51,31	25,94	23,01	23,56	23,06	24,09	23,56	24,35	25,27	25,07	24,8	24,94	24,94	24,88	23,14	23,14
SmoPG4	20,81	20,4	18,28	18,56	21,07	19,06	18,8	18,97	18,97	19,83	20,33	20,6	19,27	19,33	20	20	21,43	21,71	50,55	50,55	100	96,4	23,92	23,01	24,26	24,01	24,88	24,82	24,35	25,14	26,82	26,56	25,19	25,19	25,31	24,07	23,81
SmoPG19	20,68	20,29	18,46	18,73	21,75	19,22	18,96	18,62	18,62	20,55	20,49	20,75	19,55	19,61	20,22	20,22	22	22,29	50,87	51,31	96,4	100	24,05	23,01	24,38	24,14	24,88	24,58	23,97	25,41	27,08	26,82	25,12	25,12	25,43	24,34	24,07
YePG	18,41	17,97	21,68	21,14	18,43	19,31	19,06	19,02	19,02	22,89	19,21	19,47	20,33	20,39	21,75	21,75	20,73	21,01	25,69	25,94	23,92	24,05	100	26,08	24,41	24,41	22,89	21,92	25,53	26,13	25,31	25,06	24,48	24,48	25,54	23,04	22,79
BlPG	21,5	22,16	23,23	22,66	22,51	21,33	21,33	20,56	20,56	24,72	19,22	19,5	21,65	21,71	23,2	23,2	23,65	24,22	22,74	23,01	23,01	23,01	26,08	100	31,44	31,44	29,52	28,24	29,02	29,02	29,43	29,69	27,88	27,88	28,21	29,16	29,67
SmoPG1	27,41	26,5	23,64	23,91	26,41	26,65	26,4	25,7	25,45	27,06	25,13	25,39	25,56	25,63	29,33	29,33	29,94	29,94	23,31	23,56	24,26	24,38	24,41	31,44	100	98,5	44,39	44,23	45,15	46,3	49,18	48,94	47,02	47,02	42,99	44,78	45,01
SmoPG6	27,11	26,23	23,91	24,18	26,41	26,9	26,65	25,45	25,19	26,79	25,13	25,39	25,56	25,63	29,07	29,07	29,66	29,66	22,81	23,06	24,01	24,14	24,41	31,44	98,5	100	44,62	44,66	44,7	45,82	48,71	48,47	47,25	47,25	43,21	44,55	44,78
AtPGF7	26,41	26,46	22,44	22,16	24,08	21,77	21,77	23,51	23,26	27,3	21,64	21,9	23,96	24,02	22,93	22,93	25,71	24,86	23,84	24,09	24,88	24,88	22,89	29,52	44,39	44,62	100	65,52	44,29	44,93	47,49	47,97	47,85	47,74	47,15	47,65	47,89
AtPGF12	24,72	24,61	23,08	22,8	24,1	21,8	21,8	22,34	22,08	24,54	25,07	25,33	24,79	24,58	25,99	25,99	23,73	23,73	23,32	23,56	24,82	24,58	21,92	28,24	44,23	44,66	65,52	100	41,26	42,96	48,49	48,26	46,37	46,27	48,68	46,71	46,94
SmoPG7	26,38	25,89	21,64	21,64	20	21,34	21,34	21,5	21,5	23,48	22,02	22,28	26,26	26,61	26,88	26,88	26,14	26,42	24,87	24,35	24,35	23,97	25,53	29,02	45,15	44,7	44,29	41,26	100	99,53	51,18	50,94	51,72	51,72	48,17	47,21	46,98
SmoPG16	27,55	26,96	21,85	21,85	20,88	22,28	22,01	22,1	22,1	24,03	22,01	22,28	26,26	26,61	27,03	27,03	26,14	26,42	25,54	25,27	25,14	25,41	26,13	29,02	46,3	45,82	44,93	42,96	99,53	100	51,68	51,44	52,83	52,83	49,53	48	47,76
SmoPG2	26,17	25,22	23,06	23,06	25,34	24,8	24,53	23,53	23,8	26,74	25,2	25,75	26,11	26,18	29,08	29,08	27,48	28,05	25,07	25,07	26,82	27,08	25,31	29,43	49,18	48,71	47,49	48,49	51,18	51,68	100	97,95	55,22	55,09	53,9	54,8	55,04
SmoPG3	25,86	24,93	23,33	23,33	25,07	24,8	24,53	22,99	23,26	26,74	25,2	25,75	26,11	26,18	29,08	29,08	27,48	28,05	24,8	24,8	26,56	26,82	25,06	29,69	48,94	48,47	47,97	48,26	50,94	51,44	97,95	100	54,99	54,86	53,67	54,57	54,8
SmoPG5	27,2	26,13	23,33	23,61	23,26	24,22	23,7	22,11	22,11	25,46	21,87	21,87	25,49	25,56	27,01	27,01	26,78	26,78	25,19	24,94	25,19	25,12	24,48	27,88	47,02	47,25	47,85	46,37	51,72	52,83	55,22	54,99	100	99,79	55,41	56,09	55,86
SmoPG9	27,2	26,13	23,33	23,61	23,2	24,42	23,9	22,05	22,05	25,46	21,81	21,81	25,49	25,56	27,01	27,01	26,78	26,78	25,19	24,94	25,19	25,12	24,48	27,88	47,02	47,25	47,74	46,27	51,72	52,83	55,09	54,86	99,79	100	55,29	55,96	55,73
AtPGF10	29,08	28,69	27,12	26,85	25,46	25,71	25,45	25,9	25,9	27,57	25,07	25,07	25,35	25,14	27,27	27,27	28,81	29,1	24,38	24,88	25,31	25,43	25,54	28,21	42,99	43,21	47,15	48,68	48,17	49,53	53,9	53,67	55,41	55,29	100	56,52	56,75
SmoPG12	26,89	26,06	25,35	24,79	22,46	23,02	23,02	22,43	22,43	26,92	22,02	22,28	23,96	24,02	26,93	26,93	27,68	27,12	23,14	23,14	24,07	24,34	23,04	29,16	44,78	44,55	47,65	46,71	47,21	48	54,8	54,57	56,09	55,96	56,52	100	98,88
SmoPG13	26,59	25,78	25,07	24,51	22,73	22,75	22,75	22,69	22,69	26,65	22,28	22,55	23,68	23,74	26,67	26,67	27,97	27,4	23,14	23,14	23,81	24,07	22,79	29,67	45,01	44,78	47,89	46,94	46,98	47,76	55,04	54,8	55,86	55,73	56,75	98,88	100

Supplementary Table S2. SmoPG1 protein sequence and characterization

The signal sequence that was excluded from SmoPG1 during gene synthesis is in **orange**

Sequence type	Protein
Protein sequence	**MIAAVSKRRGFFLLWIAFFLCLFVY***Q*SNYIAQVSGSKRIARA VPRLRPVVFNLTDFGGIGDGRTINTRAFERAVAEISSAAAKS GGAQLNVPAGVWLTAPFNLTSHMTLFLEEDATILATQSEDL WPLMQPLPSYGRGRELPGPRYGSLIHGQHLEDIVITGHNGT IDGNGRKWWEKAKLKQLKHTRGRLIQFMWSRGIEISDVTLR NSPFWTVHPYDCENVTIRGVTIIAPPDAPNTDGIDPDSCRNV LIENCYISVGDDGVAVKSGWDQYGIDYGKPCANITIRNIQVN APVSAGVSIGSEMSGGITNVTVENVYIWNSKRGVRIKTTPG RGGYVTQVFYRNITMETVRVGIVIKTDYGDHPDEFYDPTALP VVEKIFFDGIYGSEVRIPARIYGSKEVPVRGLEIRDMNVGVT RKKKHVFQCSFLQGQVFGTIFPKPCEDLGTSSRPGVFREAK MTSESDGDDDA
Length	468 aa
Weight	48 kDa
N-Glycosylation sites	9
O-Glycosylation sites	7
Isoelectric point	7.64
Km	7.310 mg. mL^{-1}
Vm	1.793 $nmol.min^{-1}.\mu g^{-1}$
Yield	1 $g.L^{-1}$

Supplementary data figures captions:

Supplementary Fig. S1. Sequence alignment of SmoPG1, YePG, AtPGF10, AtPGLR.
Four sequences corresponding to PGs, SmoPG1, YePG, AtPGF10, AtPGLR were aligned. Sequences are coloured by sequence identity while signal peptide were orange squared. Amino acids corresponding to the active site are red stared.

Supplementary Fig. S2. Superposition of SmoPG1 to the structure of an endo-PG, PGLR.
SmoPG1 (pink) model superimposed to the structure of PGLR (PDB:7B7A, blue). The additional loop that is closing the SmoPG1 active site, making it an exo-PG is highlighted in dark pink.

Supplementary movie: SmoPG1-EGCG Movie MD.
MD studies of EGCG in interaction within the active site of SmoPG1.

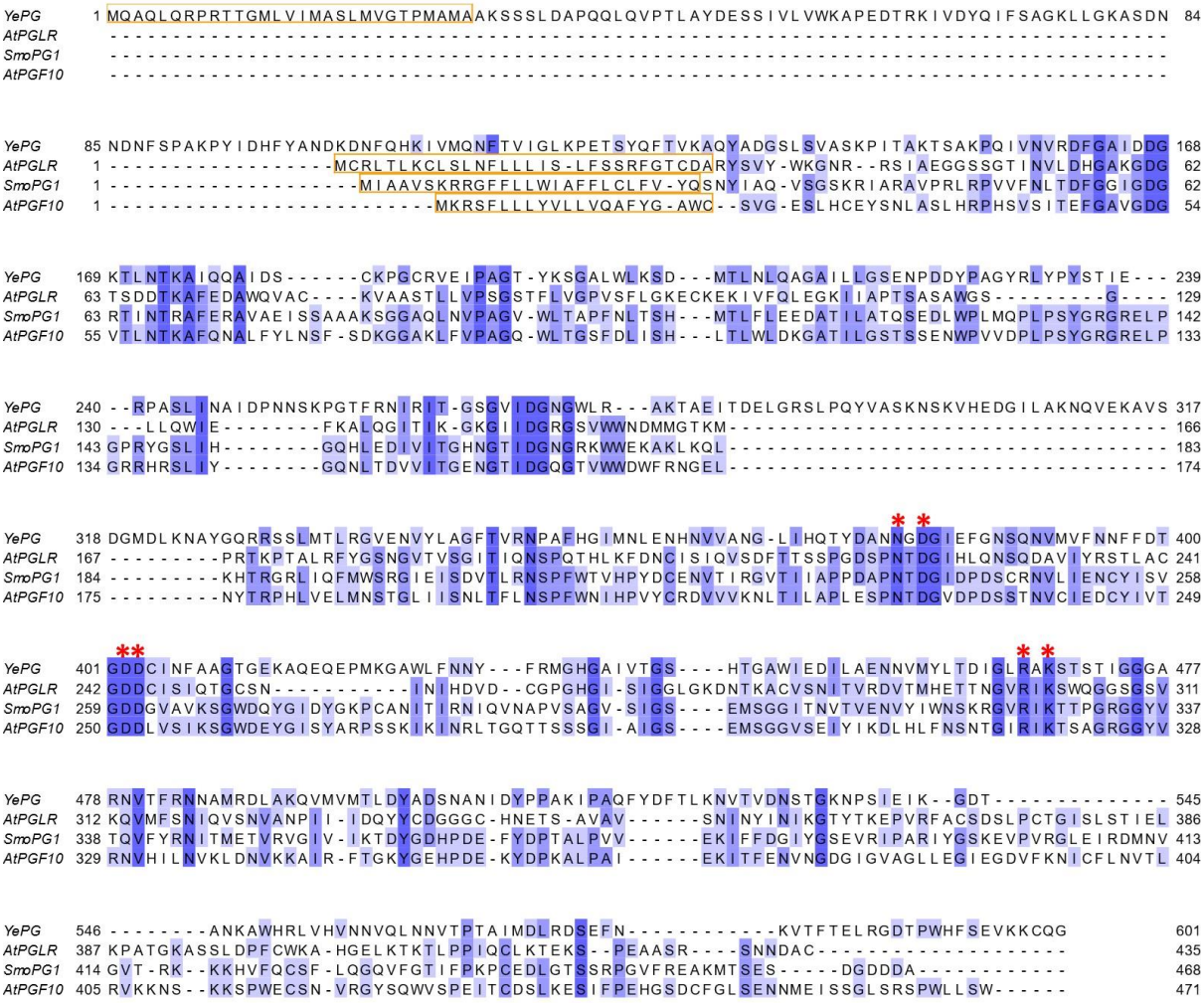

Supplementary Fig. S1

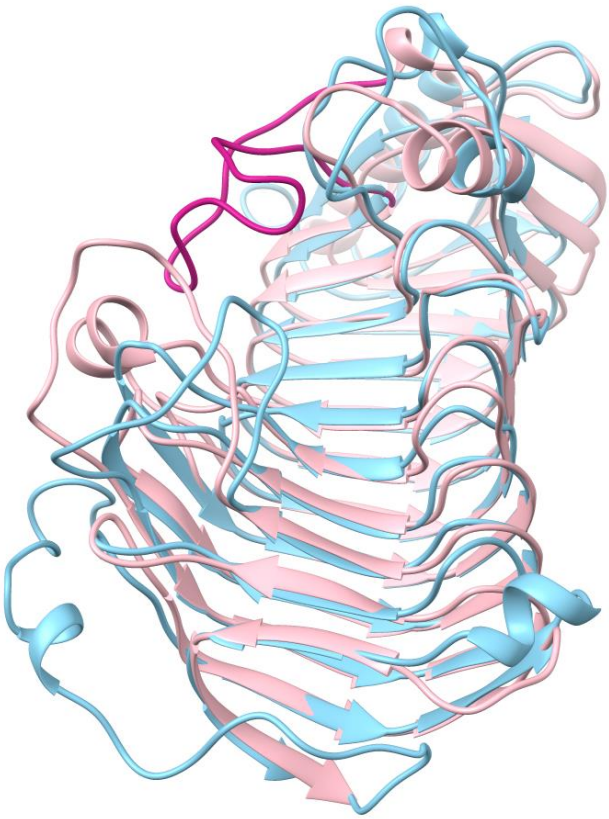

Supplementary Fig. S2